Daphnanes diterpenes from the latex of Hura crepitans L. and their PKCζ-dependent anti-proliferative activity on colorectal cancer cells

Elise Crossay, Valérie Jullian, Manon Trinel, David Sagnat, Dimitri Hamel, Emie Groppi, Corinne Rolland, Jean-Luc Stigliani, Kember Mejia, Billy Joel Cabanillas, et al.

Daphnanes diterpenes from the latex of *Hura crepitans* L. and their PKCζ-dependent anti-proliferative activity on colorectal cancer cells

Elise Crossay[a], Valérie Jullian[a], Manon Trinel[a], David Sagnat[b,c], Dimitri Hamel[b,d], Emie Groppi[a], Corinne Rolland[b], Jean-Luc Stigliani[e], Kember Mejia[f], Billy Joel Cabanillas[g], Laurent Alric[h], Etienne Buscail[b,i], Chaker El Kalamouni[j], Patrick Mavingui[j], Céline Deraison[b], Claire Racaud-Sultan[b*1], Nicolas Fabre[a*1]

[a]UMR 152 PharmaDev, Université de Toulouse, IRD, UPS, France

[b]IRSD, Université de Toulouse, INSERM, INRAE, ENVT, UPS, France

[c]Toulouse Organoids Platform, Institut de Recherche en Santé Digestive, INSERM, Toulouse, France

[d]LAAS-CNRS, Université de Toulouse, CNRS, Toulouse, France

[e]UPR 8241 LCC, Université de Toulouse, CNRS, France

[f]Instituto de Investigaciones de la Amazonia Peruana (IIAP), Iquitos, Peru

[g]Laboratorios de Investigación y Desarrollo, Facultad de Ciencias y Filosofía, Universidad Peruana Cayetano Heredia, Lima 15102, Peru

[h]Pole Digestif, Centre Hospitalier Universitaire, Toulouse, France

[i]Département de Chirurgie Digestive, Unité de Chirurgie Colorectale, Centre Hospitalier Universitaire, Toulouse, France

[j]UMR PIMIT, Université de La Réunion, INSERM U1187, CNRS 9192, IRD 249, La Réunion, France

Keywords: Euphorbiaceae, *Hura crepitans*, Daphnane diterpenes, Colorectal cancer, Caco-2 cells, Protein Kinase C

* Corresponding authors at: UMR 152 PharmaDev, Université Paul Sabatier, Faculté de Pharmacie, 35 chemin des maraichers, 31062 Toulouse, France (N. Fabre). INSERM Unité 1220, Institut de Recherche en Sante Digestive IRSD, CHU Purpan, Place du Dr Baylac, 31024 Toulouse cedex 3, France (C. Racaud-Sultan).
E-mail addresses: nicolas-fabre@univ-tlse3.fr (N. Fabre), claire.racaud@inserm.fr (C. Racaud-Sultan).
[1] These authors contributed equally to the work.

Abstract

Hura crepitans L. (Euphorbiaceae) is a thorn-covered tree widespread in South America, Africa and Asia which produces an irritating milky latex containing numerous secondary metabolites, notably daphnane-type diterpenes known as Protein Kinase C activators. Fractionation of a dichloromethane extract of the latex led to the isolation of five new daphnane diterpenes (**1**-**5**), along with two known analogs (**6**-**7**) including huratoxin. Huratoxin (**6**) and 4',5'-epoxyhuratoxin (**4**) were found to exhibit significant and selective cell growth inhibition against colorectal cancer cell line Caco-2 and primary colorectal cancer cells cultured as colonoids. The underlying mechanism of **4** and **6** was further investigated revealing the involvement of PKCζ in the cytostatic activity.

1. Introduction

Hura crepitans L. is a tree of the Euphorbiaceae, a large family with more than 3000 genus and 8000 species [1–4]. This thorn-covered tree is widespread in South America, Africa and Asia and produces an irritating milky latex containing numerous secondary metabolites, notably diterpenes [5–8]. Diterpenes found in Euphorbiaceae include more than 20 types of structures (daphnanes, ingenanes, tiglianes…) [9–11] known to possess many biological activities [3,10,12], and particularly antiviral [9,11,13–19] and antitumor properties [10]. More specifically, these diterpenes are described in the literature as activators of serine threonine protein kinases C (PKCs) [9,15,20].

PKCs are essential regulators of many cellular functions and signaling pathways, including cell proliferation, adhesion, differentiation, migration and survival [21–23]. These kinases are classified into 3 subfamilies according to their structure and mode of activation. It can be distinguished conventional diacylglycerol (DAG)- and calcium-dependent PKCs (cPKCs α, β and γ), novel calcium-independent PKCs (nPKCs θ, ε, η and δ) and atypical DAG- and calcium-independent PKCs (aPKCs λ/ι and ζ) [21,22,24]. Atypical PKCs mainly differ from the others by the fact that they can interact with phosphatidylinositol triphosphate (PIP_3) or ceramides [22], and are particularly involved in epithelial cell polarity, cytoskeleton reorganization and tissue identity [25–31]. PKCs isozymes are deregulated in many pathologies [21,22,32,33], including cancer [21,22]. More specifically, they are involved in cell transformation, tumor progression and metastasis in different types of cancer, and are particularly downregulated in colorectal cancer [21,22].

Colorectal cancer (CRC) is a global health problem. It is the third most diagnosed cancer and the second most deadly worldwide with more than 900,000 deaths in 2020 [34,35]. At an advanced stage, the 5-year survival of patients is only 40-50% and at the metastatic stage, the 5-year survival decreases to 5-15% [36] due to the proliferative and invasive capabilities of malignant cells [37]. These abilities strongly depend on PKCs and their signaling partners including β-catenin, Glycogen Synthase Kinase 3β (GSK3β), Akt and Mitogen-Activated Protein Kinase Kinase MEK [24,38–49]. To date, there is a growing interest in the development of innovative therapies targeting such signaling pathways. Notably, restoration of PKCs functions that are downregulated in CRC would be a relevant strategy to control normal adhesion, proliferation and differentiation of intestinal epithelial cells [22].

In a previous phytochemical analysis, our group identified daphnane-type diterpenes and cerebrosides as the main components of an ethanolic extract of the latex of *H. crepitans* [8]. Bio-guided fractionation revealed an interesting selective cytostatic activity of huratoxin, a mono-esterified daphnane, on human colorectal cancer cells Caco-2 with 25% of growth inhibition [50]. This antiproliferative activity was accompanied by morphological changes in Caco-2 cells. At 1.0 µg/mL, we found that huratoxin induced cytoskeleton reorganization in Caco-2 cells and the formation of structures mimicking the intestinal crypt architecture, suggesting a recovery of normal tissue differentiation [50]. Interestingly, in contrast with 12-*O*-tetradecanoylphorbol-13-acetate (TPA), a DAG-mimetic agent known to be cytotoxic for Caco-2 cells, huratoxin inhibited GSK3β and Akt [50], suggesting that huratoxin could display a specific activity on PKCs isozymes.

In this paper, we describe the isolation and structural elucidation of five new analogs of huratoxin (6'*R*-hydroxy-huratoxin (**1**), 4'*S*,5'*S*-dihydroxy-huratoxin (**2**), 4'(*Z*)-6'-oxo-huratoxin (**3**), 4'*S*,5'*S*-epoxy-huratoxin (**4**), and huratoxigenin-20-(11'-methyloctadec-12'-enoate) (**5**)) along with two known daphane-type diterpenes (huratoxin (**6**) and 6'-oxo-huratoxin (**7**)) from the latex of *H. crepitans* (Fig. 1). The cytostatic activity of compounds **1-7** on Caco-2 cells was assessed leading to structure-activity relationships. In an attempt to further investigate the mechanism of action of isolated compounds, we examined the involvement of PKCα (conventional PKC), PKCδ (novel PKC) and PKCζ (atypical PKC) previously shown to regulate Caco-2 cell proliferation (REFS 56, 59, 44, 60), on morphological and cytostatic properties of mono-esterified daphnanes. Finally, we evaluated the cytotoxic activity of the two most active daphnanes in the preclinical model of human primary colorectal cancer cells cultured as colonoids.

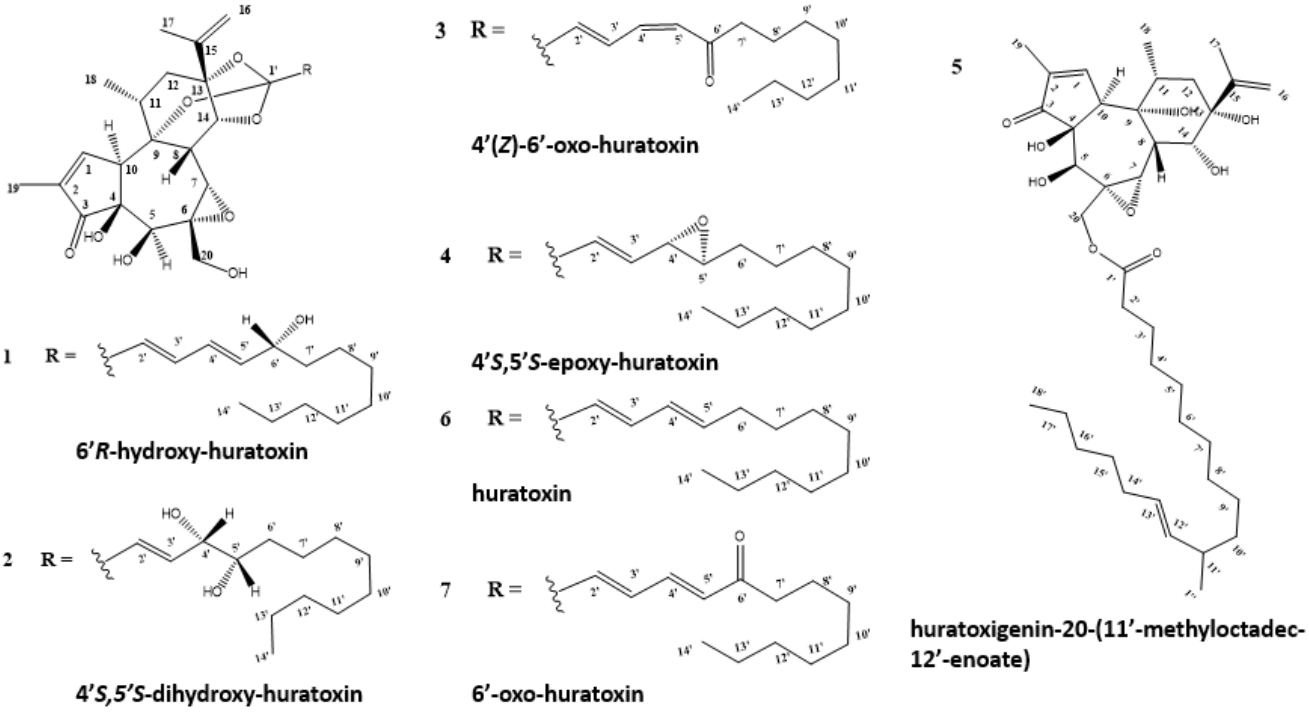

Figure 1: Structure of isolated mono-esterified daphnanes

2. Results and discussion

2.1 Isolation and structure elucidation of mono-esterified daphnanes from the latex of Hura crepitans.

A semi-quantitative analysis of the CH_2Cl_2 n°1 crude extract of the latex by UHPLC-DAD-HRMS revealed that huratoxin and its isomer represented 20.5% of the mono-esterified daphnanes against 60.0% in our previous investigation [50]. This can be explained by the presence of more polar (oxygenated) daphnane-type diterpenoids detected between 1.46 and 2.45 min by reversed-phase separation as depicted in Fig. S1 (supporting informations, SI). The qualitative analysis of the detected polar peaks, and particularly MS/MS profiles revealing diagnostic ions at m/z 361 et m/z 253 (base peak), confirm their daphnane-type structure [8] (Fig. S2).

Separations using a combination of MPLC, normal- and reversed-phase silica column chromatographies and semi-preparative HPLC afforded seven daphnane type diterpenes (**1**–**7**), among them five new derivatives (**1**-**5**) (Fig. 1). The ^{1}H and ^{13}C NMR data in Table 1 indicated that compounds **1**-**4** are orthoesterified daphnanes as ascertained by chemical shift for C-1' near δ_C 116, while **5** is an esterified daphnane as indicated by the characteristic resonance at δ_C 175.7 for C-1'.

Compound **1** was isolated as a colorless oil. Its molecular formula was established as $C_{34}H_{48}O_9$ by positive HRAPCIMS (*m/z* 601.3361 $[M+H]^+$). The IR absorptions revealed the presence of hydroxy groups (3446 cm^{-1}), α,β-unsaturated ketone (1697 cm^{-1}) and double bonds (1631 cm^{-1}) (Fig. S9). The ^1H and ^{13}C NMR data showed the presence of characteristic resonances for an isopropenyl moiety at δ_H 4.91 (H-16a), δ_H 5.0 (H-16b), δ_H 1.78 (H_3-17) and at δ_C 146.7 (C-15) and two methyl groups at δ_H 1.15 (H_3-18) and δ_H 1.78 (H_3-19), consistent with a daphnane-type structure. The signals of the typical orthoester carbon at δ_C 116.4 (C-1') and an oxygenated methylene at δ_H 3.77 (H-20a) and δ_H 3.81 (H-20b) suggested that **1** is an orthoesterified daphnane-type diterpenoid. Other resonances due to polyoxygenated functionalities in the daphnane skeleton were observed for an epoxy group at δ_H 3.40 (H-7), δ_C 61.1 (C-6), δ_C 64.3 (C-7), one oxygenated methine at δ_C 72.1 (C-5) and one oxygenated tertiary carbon at δ_C 72.7 (C-4). The positions of these functionalities were deduced by analyses of 2D-NMR HSQC, COSY and HMBC spectra where key correlations are shown in Fig. 2A. The HMBC cross peak observed between H-14 (δ_H 4.44) and C-1' confirms the position of the orthoesterified side chain. The ^{13}C signals of four ethylenic carbons at δ_C 125.9 (C-2'), δ_C 134.0 (C-3'), δ_C 128.5 (C-4') and δ_C 140.7 (C-5'), combined with COSY correlations, show the presence of two conjugated double bonds on the side chain and their *E*-configurations were deduced from the ^1H NMR coupling constants $J_{2',3'}$=15.5 Hz and $J_{4',5'}$= 15.3 Hz. ^1H-^1H COSY cross-peak between H-5' at δ_H 5.89 and the low-field H-6' at δ_H 4.16 revealed the presence of an oxygenated methine for C-6'. The rest of the alkyl chain consists of seven methylene groups at δ_C 37.7 (C-7'), δ_C 27.7 (C-8'), δ_C 29.7-30.0 (C-9' to C-11'), δ_C 32.3 (C-12'), δ_C 23.1 (C-13') and one methyl group at δ_C 14.3 (C-14') that have been assigned according to their HMBC correlations (Fig. 2A) and by comparison with literature [50]. Furthermore, NOESY correlations observed in the daphnane core (Fig. 2B) and ECD spectrum (Fig. S10) of compound **1** were similar to those of huratoxin (**6**) allowing us to determine the absolute configuration of the diterpene skeleton. In order to determine the configuration of the C-6', Gauge-Independent Atomic Orbital (GIAO) NMR chemical shifts calculations supported by the advanced statistical method DP4+ [51] was performed on the structure of **1** with the two possible configurations at C-6'. In this approach, the differences between *ab initio* computed ^{13}C and ^1H NMR scaled chemical shifts and experimental data are considered (Figs. S11 and S12). Then, the probability of the error in each chemical shift of each configuration is computed using Student *t*-test. The product of these probabilities divided by the sum of the probabilities gives the DP4+ probability for each configuration (Fig. S13).

DP4+ calculations give a probability of 99.1% for the 6'*R* configuration. Thus, **1** was named 6'*R*-hydroxy-huratoxin (Fig. 1).

Compound **2** was isolated as a colorless oil. Its molecular formula was established as $C_{34}H_{50}O_{10}$ by positive HRAPCIMS (*m/z* 619.3475 $[M+H]^+$) and differed by 18 u when compared to **1**. The IR absorptions revealed the presence of hydroxy groups (3384 cm^{-1}), α,β-unsaturated ketone (1701 cm^{-1}) and double bonds (1634 cm^{-1}) (Fig. S20). All of the characteristic chemical shifts of the daphnane skeleton were present on ^{1}H and ^{13}C NMR spectra of **2**. As for **1**, the key HMBC correlation detected between H-14 at δ_H 4.40 and C-1' at δ_C 116.6 confirmed the same position of the orthoesterified side chain. The difference with compound **1** is therefore located on the alkyl chain where the resonance of only two ethylenic carbons at δ_C 125.9 (C-2') and δ_C 135.3 (C-3') revealed the presence of one double bond in *E*-configuration deduced from the coupling constant $J_{2',3'}$=15.7 Hz. ^{1}H-^{1}H COSY cross peaks observed between H-3' (δ_H 6.29)/H-4' (δ_H 4.00) and H-4' (δ_H 4.00)/H-5' (δ_H 3.50) allowed us to assign two oxygenated methine groups at positions C-4' and C-5' (Fig. 2A). Thus, the planar structure of **2** was determined. The relative configuration of the daphnane skeleton of **2** was deduced to be the same than as **1** since it presented the same key NOESY correlations (Fig. 2B). Although the ECD spectrum of **2** was different than these of huratoxin (Fig. S21), we assumed that the absolute configuration of the daphnane core was the same in the two molecules. Indeed, in previous studies [50,52] the absolute configuration of the daphnane core has always been described to be identical to that of huratoxin. Free rotation of the side chain makes difficult the determination of the configuration of the C-4' and C-5' stereocenters. However, GIAO NMR chemical shifts calculations were performed on the structure of the compound **2** (Figs. S22 and S23) for the four diastereoismers (4'*S*-5'*S*, 4'*R*-5'*R*, 4'*S*-5'*R* and 4'*R*-5'*S*). The comparison with experimental NMR shifts of **2** was in favor of the 4'*S*-5'*S* configuration with a DP4+ calculation showing a probability of 99.6% (Fig. S24). Thus, **2** was named 4'*S*,5'*S*-dihydroxy-huratoxin (Fig.1).

Compound **3** was isolated as a colorless oil. Its molecular formula was established as $C_{34}H_{46}O_9$ by positive HRAPCIMS (*m/z* 599.3205 $[M+H]^+$) which corresponded to the molecular formula of a previously isolated daphnane orthoester identified to 6'-oxo-huratoxin [50] and also isolated in this work (compound **7**). The comparison of ^{1}H and ^{13}C NMR data of these two isomers displayed differences only located on the orthoester side chain and notably on the C-3' double bond. The major difference concerned the $J_{3',4'}$ coupling constant

measured to be 11.4 Hz for compound **3** instead of 15.6 Hz for **7**, thus indicating a *Z*-configuration for the C-3'/C-4' double bond. The absolute configuration of **3** was drawn as depicted in Fig. 1 according to NOESY correlations that were superimposable to those of compounds **1**-**2** (Fig. 2B) and similar ECD spectrum to 6'-oxo-huratoxin (Fig. S32) [50]. Therefore, **3** was named 4'(*Z*)-6'-oxo-huratoxin.

Compound **4** was isolated as a colorless oil. Its molecular formula was established as $C_{34}H_{48}O_9$ by positive HRAPCIMS (*m/z* 601.3367 $[M+H]^+$). The IR absorptions revealed the presence of hydroxy groups (3421 cm^{-1}), α,β-unsatured ketone (1701 cm^{-1}) and double bonds (1632 cm^{-1}) (Fig. S45). The analysis of NMR spectra confirmed the presence of a daphnane skeleton. Moreover, we noticed characteristic chemical shifts of another epoxy group at δ_C 57.4 and 61.1. HMBC correlations between C-1' (δ_C 115.7) and a multiplet at δ_H 6.00 (H-2' and H-3') allowed us to assign a double bond between C-2' and C-3' (Fig. 2A). Additionally, ^{1}H-^{1}H COSY cross peaks among H-3' (δ_H 6.00)/H-4' (δ_H 3.13) and H-4'/H-5' (δ_H 2.85) helped to locate the epoxy group at C-4', C-5' (Fig. 2A). Thus, compound **4** was identified as 4',5'-epoxy-huratoxin (Fig. 1). ^{1}H-NMR multiplicities of H-2' (δ_H 6.00) and H-3' (δ_H 6.00) appearing as multiplets, a ^{1}H-NMR spectrum of **4** was recorded in benzene d_6 and permitted to separate these protons and to measure their coupling constant ($J_{2',3'}$ = 15.7 Hz (Fig. S44)), thus indicating *E*-configuration. The relative configuration of the daphnane core of **4** was determined to be the same than precedent compounds **1**-**3** according to the analysis of NOESY correlations (Fig. 2B). Due to similarity of ECD spectra of **4** and **2**, it was also assumed that daphnane skeleton of **4** has the same absolute configuration than previous isolated compounds (Fig. 1). Thanks to GIAO NMR chemical shits calculation on the structure of compound **2** (Figs. S47 and S48), 4'*S*,5'S was deduced to be the most likely configuration of the side chain of **4**. Indeed, DP4+ calculation showed a probability of 99.6% in favor of this hypothesis when compared to the 4'*R*-5'*R*, 4'*R*-5'*S* and 4'*S*-5'*R* candidates. (Fig. S49). Thus, **4** was identified as 4'S,5'*S*-epoxy-huratoxin (Fig. 1).

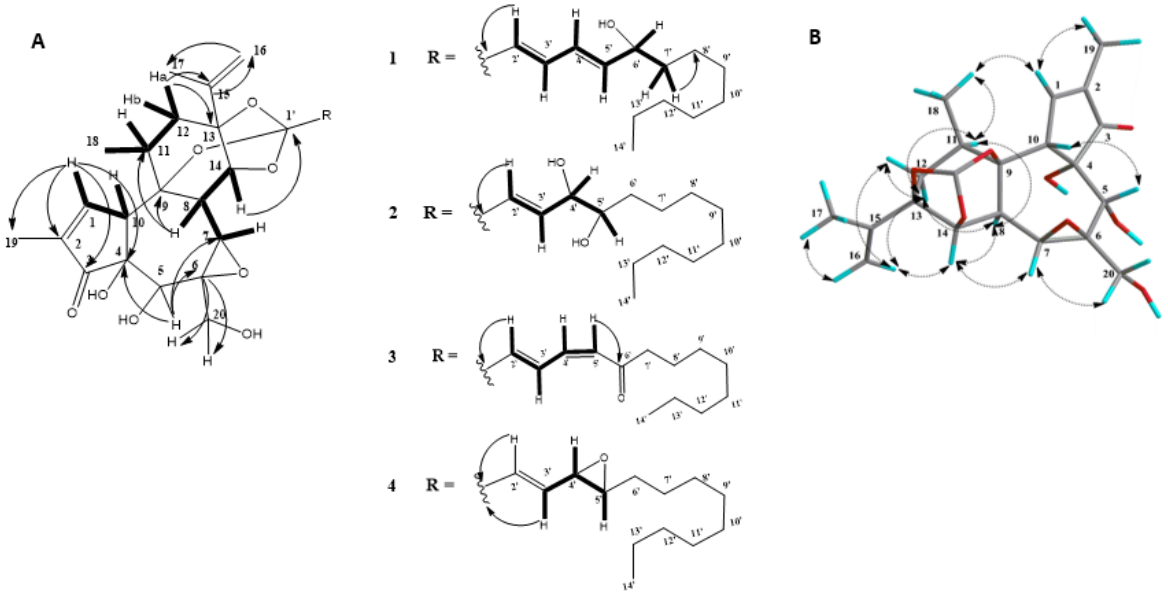

*Figure 2:A) Key COSY (bold) and HMBC (arrow) correlations of compounds **1-4**. B) Key NOESY correlations (arrow) of the daphnane core of compounds **1-4***

Compound **5** was isolated as a colorless oil. Its molecular formula was established as $C_{39}H_{62}O_9$ by positive HRAPCIMS (*m/z* 675.4455 $[M+H]^+$). The IR absorptions were the same as for the precedent compounds described in this work (Fig. S56). The assignment of carbons and protons constituting the daphnane core was performed through the analysis of 1D and 2D NMR spectra. However, when compared to NMR spectra of compounds **1**-**4**, some small differences can be noted in the chemical shifts of certain atoms of the daphnane core and particularly C-6 (δ_C 78.3) and C-7 (δ_C 80.8) that were deshielded, whereas H-5 (δ_H 3.64) resonated at higher field. So, the electronic environment around these atoms is modified when compared to compounds **1**-**4**. The HMBC cross peak observed between H_2-20 (δ_H 4.34 and 4.44) and C-1' (δ_C 175.7) explained this observation since it revealed that **5** was esterified at C-20 (δ_C 66.2) (Fig. 3A), in contrast to other mono-esterified daphnanes previously isolated from *H. crepitans*. It is worth mentioning that the resonances of C-13 at δ_C 74.7 and C-14 at δ_C 77.8 were also shielded. This finding is consistent with the literature in which Otsuki *et al*., in 2020, reported the isolation and structural elucidation of non-(ortho)esterified daphnane-type diterpenes showing similar chemical shifts for carbons 9, 13, and 14 [53]. Furthermore, none of the signals in the ^{13}C NMR spectrum could be assigned as an orthoester quaternary carbon. Concerning the structure of the C-20 ester chain, a neutral loss of 296 u observed in the MS^2 spectrum (Fig. S2) of **5** obtained from the $[M+H]^+$ ion at m/z 675 permitted to deduce a 19 carbons alkyl chain with 1 index of hydrogen deficiency. HMBC cross peak between a triplet at δ_H 2.39 (H-2') and C-1' (δ_C 175.7) and ^1H-^1H COSY correlation between

H-2’ and H-3’ (δ_H 1.59) allowed to assign the signals of C-2’ (δ_C 34.7) and C-3’ (δ_C 25.4). H-3' correlates, in the HMBC spectrum, with a cluster of 6 carbons located between δ_C 29.5 and 30.1 and assigned to carbons C-4' to C-9'. The methyl signal [δ_H 0.88 (t, *J* = 6.7), δ_c 14.3] is characteristic of a terminal methyl (C-18’). H_3-18’ correlates in the COSY spectrum with a large signal at δ_H 1.26, itself correlating, in the HSQC spectrum, with several methylene ^{13}C signals, whose signals at δ_c 23.1, 27.7, and 32.3. According to the literature, these ^{13}C chemical shifts are characteristic of methylenes located at the end of an alkyl chain [50] and were therefore positioned at δ_C 23.1 for C-17', δ_C 32.3 for C-16' and δ_C 27.7 for C-15'. The resonances of two ethylenic carbons at δ_C 129.9 and δ_C 136.8, bearing protons at δ_H 5.36 (dd, *J* = 15.6, 6.8) and δ_H 5.25 (dd, *J* = 15.6, 7.5) respectively, confirmed the presence of a double bond in *E*-configuration on the side chain. The HMBC correlation of the two ethylenic protons with a methyne signal at δ_C 33.0 and a methylene at δ_C 37.1, bearing protons at δ_H 1.97 (q, *J* = 6.8) and δ_H 2.02 (m), respectively, allowed to characterize the two allylic positions. Furthermore, a doublet [δ_H 0.94 (d, *J* = 6.7)], borne by a methyl carbon (δ_C 21.1) indicates the presence of a branched methyl group on the chain (CH_3-1’’). This doublet correlates, in the COSY spectrum, with the signal at δ_H 2.02 corresponding to an allylic proton. So, all the 19 carbons of the chain have been assigned and a CH_2-CH(CH_3)-CH=CH-CH_2 moiety can be positioned between C-9’ and C-15’ but remains to be located. Unfortunately, the superposition of the NMR signals did not allow us to discriminate between the two possible structures for this molecule as drawn in Fig. 4. However, GIAO NMR chemical shifts calculations have been made for the two fatty methyl esters mimicking the two candidates of C-20 esterified side chains of compound **5** (Fig. S58). The comparison between calculated and experimental NMR shifts of **5** was in favor of a 11’ methyl branching and 12’,13’ unsaturation. Indeed, the DP4+ calculation (Figs. S59 to S61) showed an unambiguous probability of 100% for the structure n°1 of **5** depicted in Fig. 1. As drawn (Fig. 1), the basic daphnane diterpene core of **5** is the same that of huratoxin (*i.e.* 1,3-α,β-unsaturated-ketone-4,5,9,13,14,20-hexahydroxy-6,7-epoxy-daphnane) which we propose to call “huratoxigenin” as in one of our earlier articles [8]. Consequently, the trivial name huratoxigenin-20-(11’-methyloctadec-12’-enoate) was chosen for compound **5**. The NOESY correlations observed for **5** in the daphnane core were similar to the above compounds, allowing the determination of its relative configuration (Fig. 3B). Thus, the structure of **5** was determined as shown in Fig. 1.

N°	1	2	3	4	5

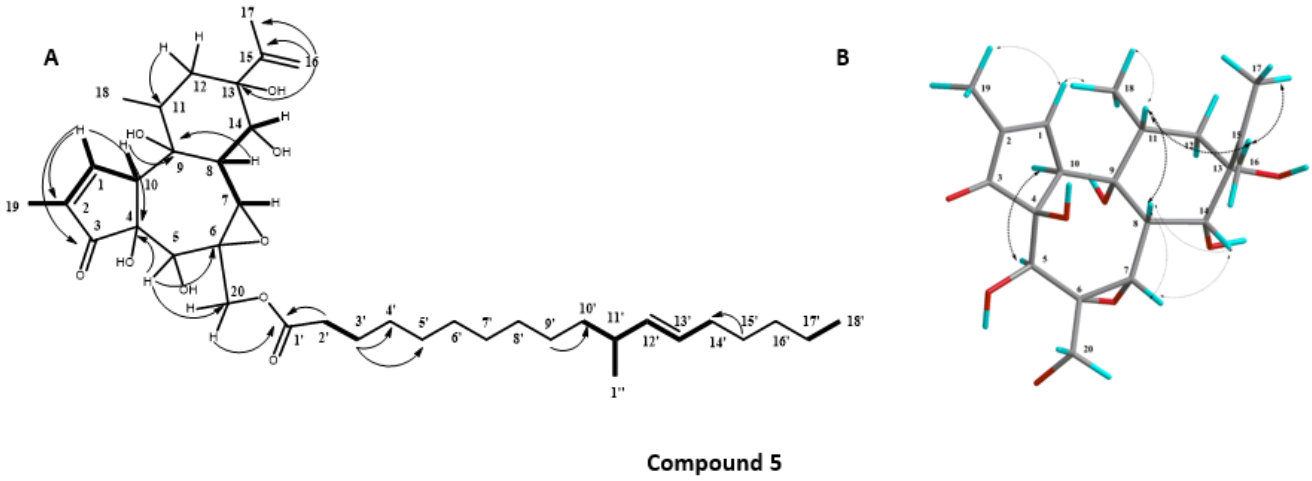

*Figure 3: A) Key COSY (bold) and HMBC (arrow) correlations of the compound **5**. B) Key NOESY correlations (arrow) of the esterified daphnane core of compound **5**.*

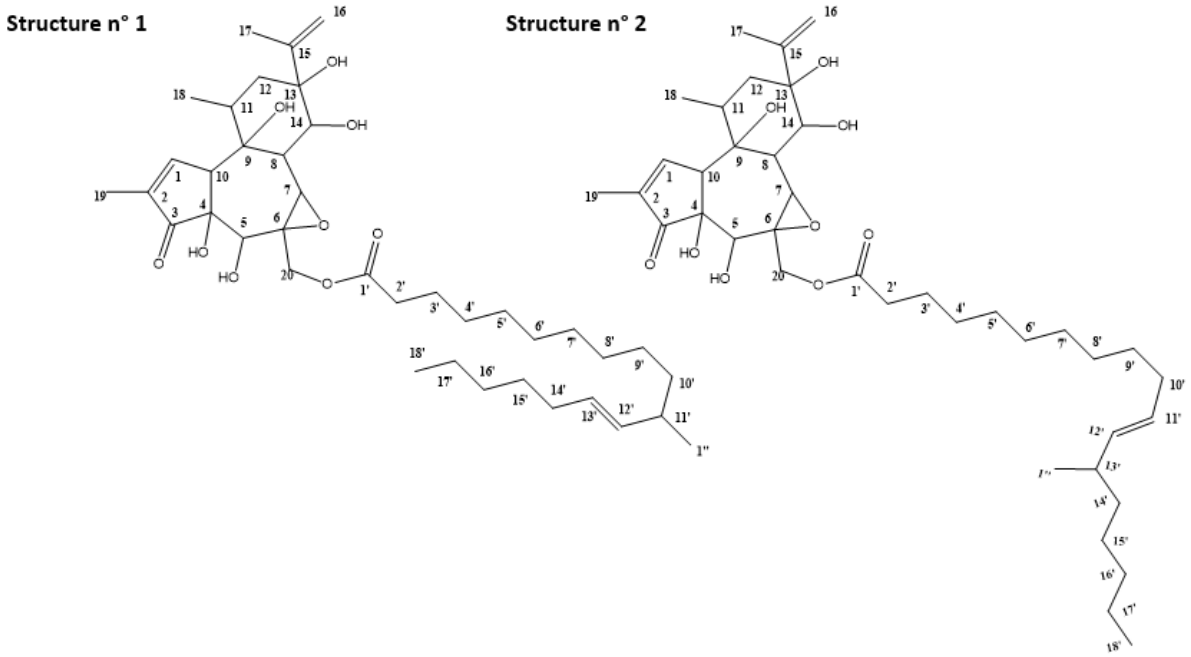

*Figure 4: Proposal of structures for compound **5**.*

Huratoxin **(6)** and 6'-oxo-huratoxin **(7)** (Fig. 1) were identified by comparison of their spectroscopic data with previous work [50]. Their NMR data are presented in Figs. S62 to S64 and Table S1 in supporting information.

	δ_H (*J* in Hz)	δ_C	δ_H (*J* in Hz)	δ_C	δ_H (*J* in Hz)	δ_C	δ_H (*J* in Hz)	δ_C	δ_H (*J* in Hz)	δ_C
1	7.61 ; m	161.1	7.48 ; s	160.3	7.60 ; m	161.0	7.59 ; m	161.0	7.67 ; m	162.1
2	-	137.3	-	137.4	-	137.3	-	*137.2*	-	135.1
3	-	210.0	-	209.7	-	210.0	-	210.0	-	209.8
4	-	72.7	-	73.6	-	72.7	-	72.7	-	75.0
5	4.25 ; s	72.1	4.08 ; s	71.0	4.26 ; s	72.2	4.24 ; bs	72.2	3.64 ; s	72.6
6	-	61.1	-	62.3	-	61.0	-	61.0	-	78.3
7	3.40 ; s	64.3	3.31 ; s	64.3	3.42 ; s	64.2	3.39 ; s	64.3	3.94 ; m	80.8
8	2.95 ; d (2.5)	37.1	2.91 ; d (2.4)	37.1	2.97 ; d (2.5)	37.1	2.95 ; d (2.6)	37.1	2.91 ; m	38.8
9	-	80.1	-	80.6	-	80.4	-	*80.2*	-	79.0
10	3.77 ; m	48.5	3.73 ; m	48.8	3.77 ; m	48.4	3.75 ; m	48.4	3.64 ; m	53.5
11	2.49 ; m	35.3	2.48 ; m	35.4	2.48 ; m	35.4	2.48 ; m	35.3	2.20 ; m	37.3
12a	1.65 ; d (14.4)	36.8	1.54 ; d (14.4)	36.9	1.65 ; d (14. 4)	36.8	1.62 ; s	36.8	1.83 ; m	38.1
12b	2.24 ; dd (14.4 ; 8.6)		2.20 ; dd (14.4 ; 8.6)		2.25 ; dd (14.4 ; 8.6)		2.23 ; m		2.20 ; dd (14.4 ; 8.6)	
13	-	85.0	-	85.3	-	85.3	-	*85.3*	-	74.7
14	4.44 ; d (2.5)	82.3	4.40 ; d (2.3)	82.7	4.47 ; d (2.5)	82.4	4.44 ; d (2.6)	82.3	4.15 ; d (3.7)	77.8
15	-	146.7	-	147.1	-	146.5	-	*146.4*	-	145.7
16a	4.91 ; m	111.2	4.83 ; s	111.1	4.92 ; m	111.3	4.90 ; m	111.2	5.02 ; s	114.3
16b	5.02 ; bs		4.96 ; s		5.04 ; m		5.01 ; m		5.08 ; s	
17	1.78 ; m	19.2	1.72 ; bs	19.0	1.79 ; m	19.2	1.77 ; m	*19.2*	1.78 ; s	19.1
18	1.15 ; d (7.1)	20.5	1.09 ; d (7.0)	20.4	1.17 ; d (7.1)	20.5	1.16 ; d (7.1)	*20.4*	0.99 ; d (6.7)	17.6
19	1.78 ; m	10.1	1.70 ; bs	9.90	1.79 ; m	10.1	1.76 ; m	*10.1*	1.78 ; s	9.97
20a	3.77 ; m	65.4	3.58 ; d (12.4)	65.1	3.77 ; m	65.3	3.77 ; d (12.5)	65.4	4.34 ; d (11.9)	66.2
20b	3.81 ; d (12.1)		3.87 ; d (12.4)				3.81 ; d (12.5)		4.44 ; d (11.9)	
1’	-	116.4	-	116.6	-	116.1	-	*115.7*	-	175.7
2’	5.80 ; d (15.5)	125.9	5.84 ; d (15.7)	125.9	6.10 ; d (15.6)	134.6	6.00 ; m	127.8	2.39 ; t (7.5)	34.7
3’	6.71 ; dd (15.5 ; 10.8)	134.0	6.29 ; dd (15.7 ; 6.0)	135.3	7.86 ; ddd (15.6 ; 12.6 ; 1.1)	130.7	6.00 ; m	133.9	1.59 ; m	25.4
4’	6.25 ; dd (15.3 ; 10.8)	128.5	4.00 ; m	75.0	6.43 ; ddd (12.6 ; 11.4 ; 0.7)	139.7	3.13 ; m	57.4	1.26 ; m	29.5 - 30.1
5’	5.89 ; dd (15.3 ; 6.5)	140.7	3.50 ; m	74.8	6.18 ; d (11.4)	128.0	2.85 ; m	61.1		
6’a	4.16 ; q (6.5)	72.6	1.33 ; m	32.8	-	201.6	1.62 ; s	32.4		
6’b			1.45 ; m							
7’a	1.52 ; m	37.7	1.26 ; m	26.4	2.48 ; m	44.8	1.43 ; m	26.3		
7’b			1.45 ; m							
8’	1.28 ; m	25.7	1.21 ; m	32.8	1.60 ; m	24.4	1.27 ; m	29.7		
9’		29.7	1.21 ; m	29.9 –	1.27 – 1.29 ;	29.6		–		
10’		–		30.2	m	-		29.9	1.26 ; m	37.6
11’		30.0				29.8			2.02 ; m	37.1
12’	1.28 ; m	32.3	1.21 ; m	32.5	1.29 ; m	32.3	1.27 ; m	*32.3*	5.25 ; dd (15.6 ; 7.5)	136.8
13’	1.28 ; m	23.1	1.21 ; m	23.2	1.29 ; m	23.1	1.27 ; m	23.1	5.36 ; dd (15.6 ; 6.8)	129.9
14’	0.88 ; t (6.9)	14.3	0.81 ; t (6.8)	14.1	0.88 ; t (7.0)	14.3	*0.88 ; t (7.0)*	14.3	1.97 ; q (6.8)	33.0
15’	-	-	-	-	-	-			1.26 ; m	27.7
16’	-	-	-	-	-	-			1.26 ; m	32.3
17’	-	-	-	-	-	-			1.26 ; m	23.1
18’	-	-	-	-	-	-			0.88 ; t (6.7)	14.3
1’’	-	-	-	-	-	-			0.94 ; d (6.7)	21.1

*Table 1: ^{1}H- and ^{13}C NMR data (δ in ppm) for the daphnane-type orthoesters (**1**) (CD_2Cl_2), (**2**) (CD_2Cl_2/MeOD 50/50 v/v), (**3**) (CD_2Cl_2) and (**4**) (CD_2Cl_2) and daphnane- type ester (**5**) (CD_2Cl_2).*

2.2. In vitro selective cytostatic activity of isolated mono-esterified daphnanes

As shown in our previous work [50], huratoxin exhibits cytostatic activity on Caco-2 colorectal cancer cells. To further investigate the structure activity relationships, isolated daphnanes **1-7** were evaluated for their cytotoxicity on Caco-2 cells. As previously shown for huratoxin [50], these daphnanes did not induce death of Caco-2 cells (not shown). In Fig. 5, showing the cytostatic activity of tested compounds normalized to the antiproliferative effect of huratoxin (**6**), daphnane derivatives **1-4** and **7** show cytostatic activity on Caco-2 cells while **5** was inactive. Compounds **1**, **3** and **7** have similar antiproliferative effect than huratoxin (**6**) with around 25% of growth inhibition of Caco-2 cells and confirms the results obtained for huratoxin in our previous work [50]. It is interesting to note that compounds **1**, **3** and **7** and huratoxin (**6**) are orthoesterified daphnanes with two conjugated double bonds on their alkyl chain and that the C3'/C4' double bound *Z* configuration for oxo-huratoxin (**3**) does not change the activity compared to its *E* analog (**7**). The most active derivative 4',5'-epoxy-huratoxin (**4**) is also an orthoesterified daphnane but with one of the side chain double bonds oxidized by an epoxide group. Compound **2**, which is about 25% less antiproliferative than huratoxin, has, as for **4**, an oxidized side chain double bond but by two hydroxyl groups instead of an epoxide. Finally, the not active daphnane **5** is the only non orthoesterified compound but presenting a single ester alkyl chain located at C-20. These results suggest that orthoesterified chain is necessary for the activity, as previously assumed by Trinel *et al.* [50]. Similarly, the structure of the orthoester side chain participates to the activity since conjugated double bonds and/or epoxy substitutions are necessary to the antiproliferative effect or even exalt it as shown for epoxy-huratoxin, as summarized in Fig. 6. Huratoxin (**6**) being active and the most abundant daphnane in the latex and epoxy-huratoxin (**4**) being the most active on Caco-2 cells, only those two compounds were used for further investigations. The Fig. 7 shows the dose-response effect of **4** and **6** on the proliferation of Caco-2 cells. At 0.5 µg/mL, huratoxin (**6**) reaches a plateau at 20% growth inhibition while epoxy-huratoxin (**4**) reaches 30% growth inhibition at 1.0 µg/mL, that is in good agreement with the results described for Fig. 5. The assessment of active caspase 3 under treatment of Caco-2 cells by both compounds showed no statistically significant difference compared to basal conditions (not shown), thus indicating that huratoxin and epoxy-huratoxin do not trigger an apoptotic pathway and have a cytostatic effect. In order to confirm the selectivity of huratoxin against cancer cell line [50] and evaluate that of epoxy derivatives, the two compounds were incubated with the non-cancerous human intestinal epithelial cell (hIEC6) line. As shown in Fig. 8, the non-statistical difference observed between solvent (DMSO) and tested molecules validates the selectivity of cytostatic effects of **4** and **6** against the colorectal cancerous cell.

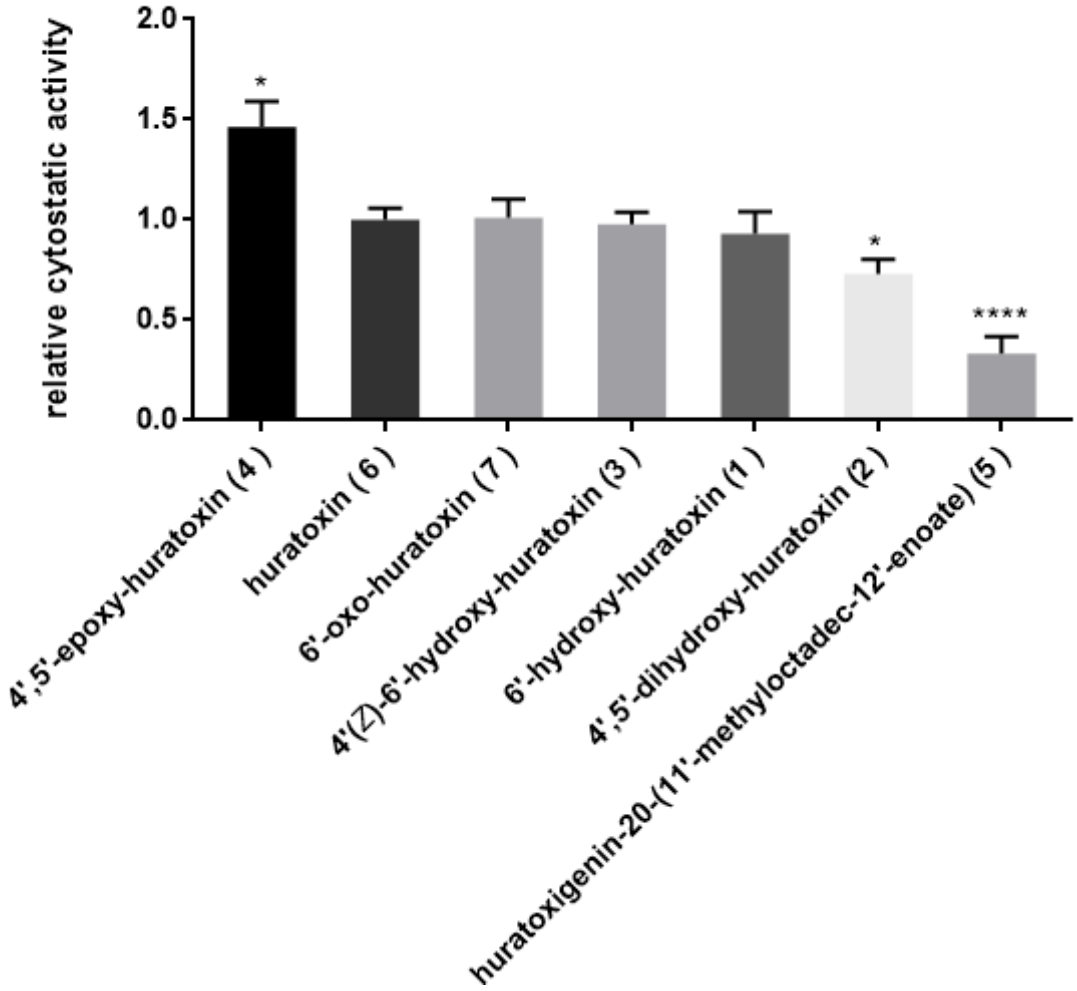

*Figure 5: Cytostatic activity of compounds **1-7** on Caco-2 cells. Cells were incubated during 48 h with mono-esterified daphnanes at 1 µg/mL, then cell viability was measured by colorimetry. The cytostatic activity of the compounds has been normalized to that of huratoxin. Mean ± S.E.M., t-test from triplicates of 1 to 6 independent experiments. *p<0.05; ****p<0.0001.*

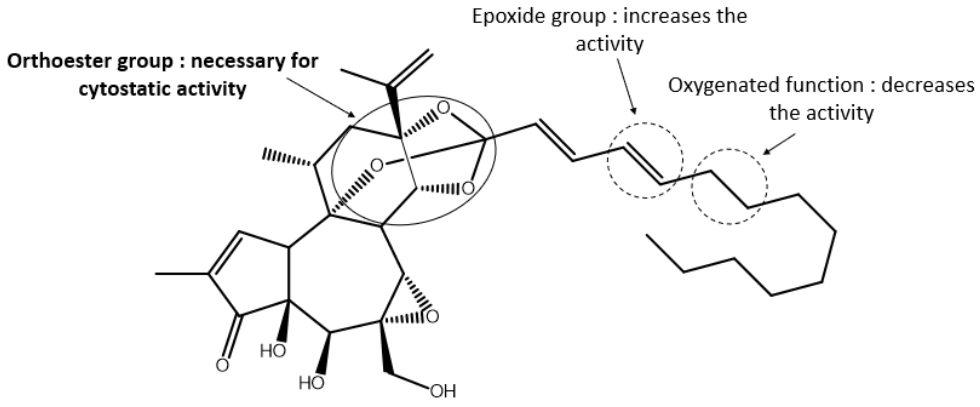

Figure 6: Structure activity relationships of mono-esterified daphnanes

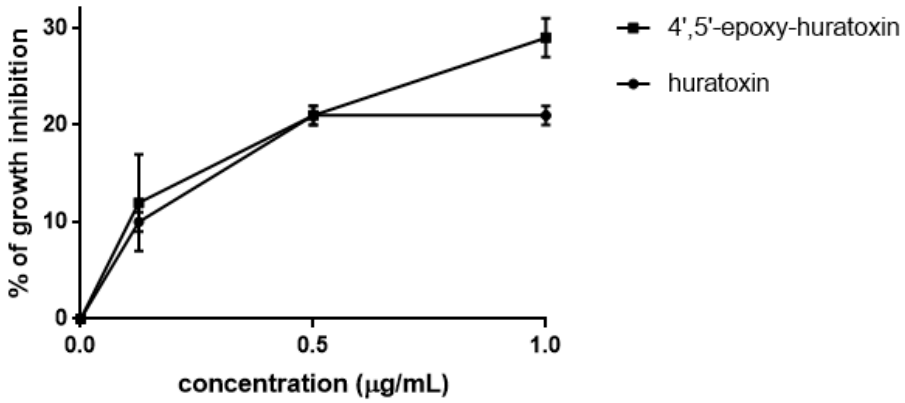

Figure 7: Cytostatic activity of huratoxin and 4',5'-epoxy-huratoxin at different concentrations. Cells were incubated with different concentrations (0.125, 0.5 and 1 µg/mL) for 48 h and cell viability was measured by colorimetry and compared to the control (DMSO). Mean ± S.E.M. from 2 independent experiments.

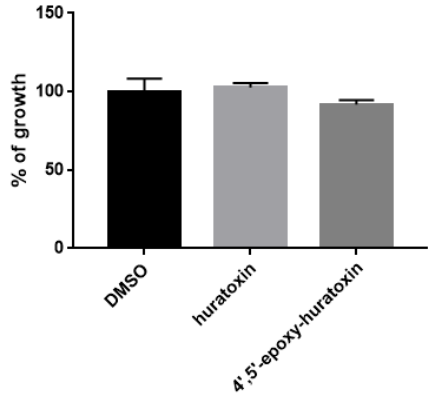

Figure 8: Impact of huratoxin and 4',5'-epoxy-huratoxin on the growth of hIEC6 cells. Cells were incubated with mono-esterified daphnanes at 1 µg/mL for 48 h then cell viability was measured by colorimetry and compared to control (DMSO). Mean ± S.E.M. t-test from 3 independent experiments: no significative differences compared to DMSO.

2.3. Morphological effects of huratoxin and 4',5'-epoxy-huratoxin on Caco-2 cells

Besides the antiproliferative activity and as shown in previous work [50] for huratoxin, the treatment of Caco-2 cells by huratoxin and its epoxy derivative caused cellular aggregates as depicted in the confocal images of nuclei and cytoskeleton labeling in Fig. 9, and this, from the dose of 0.125 µg/mL (not shown). Interestingly, the two daphnanes influence both the proliferative and adhesive capacities of intestinal epithelial cells. These abilities are particularly important to maintain homeostasis through the maturation of intestinal epithelial cells in the crypt, the regenerative unit of the intestine and colon [54]. To further analyze the changes in cellular functions induced by huratoxin and epoxy-huratoxin, fluorescent labeling of nuclei and cytoskeleton were carried out. As shown in Fig. 9 (fluorescent images observed by confocal microscopy), morphological changes are accompanied by densification of cytoskeleton in agreement with a reorganization of the architecture of the epithelial tissue.

Our previous work showed that treatment with huratoxin even caused the formation of neo-crypt [50]. The present observations are probably the first step of this process and suggest that huratoxin and 4',5'-epoxy-huratoxin could be excellent candidates for cancer therapy to restore normal tissue functions, *i.e.* controlled proliferation and differentiation that are lost during tumor transformation [55].

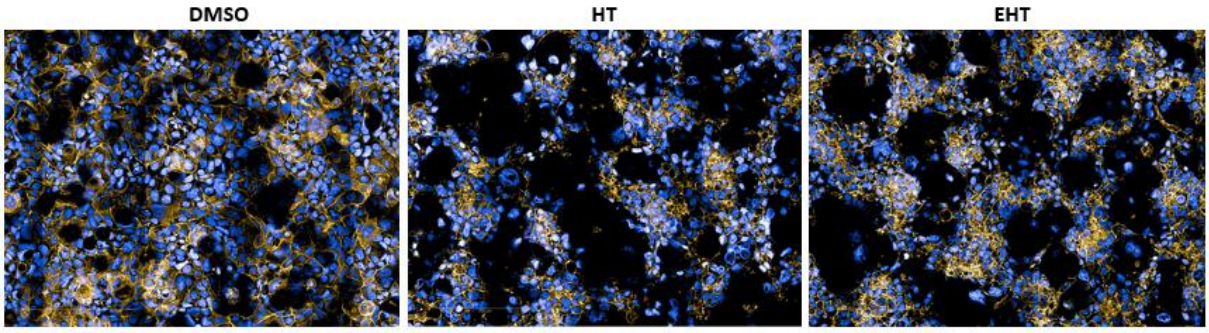

Figure 9: Morphological changes induced by the treatment of Caco-2 cells with huratoxin and 4',5'-epoxy-huratoxin. 48 h after treatment with daphnanes (huratoxin, HT; 4',5'-epoxy-huratoxin, EHT; 1 µg/mL) or their solvent DMSO (0.01%), fluorescent labeling of nuclei (hoechst, blue) and cytoskeleton (phalloidin, yellow) was performed and the results were observed by confocal microscopy (OPERA Phenix®, objective 63X, size scale= 200 µm). Photographs are representative of duplicates from one experiment.

2.4. Involvement of PKCζ in the effects of huratoxin and 4',5'-epoxy-huratoxin

Diterpenes encountered in Euphorbiaeace, including daphnane-type diterpenes, are known for their ability to activate the serine-threonine kinases PKCs. All PKC families (classic, novel, atypical) are represented [56] in Caco-2 cells. However, in our experimental conditions (confluent monolayer of Caco-2 cells), Abraham and colleagues detected the expression of only PKCα, PKCβI, PKCβII (classics), PKCδ (novel) and PKCζ (atypic) [56]. They noted that PKCγ and PKCε were not or very poorly expressed in this cell line. Also, we did not find in literature articles demonstrating the expression of PKCη in Caco-2 cells. Concerning PKCθ (novel) and PKCι (atypical), these two isoforms are expressed in Caco-2 cells and play important roles in cytoskeleton organization [57,58] but, to our knowledge, their potential role in the control of cell proliferation has not yet been described. Given that, we focused our investigations on PKCα [56], PKCδ [59], and PKCζ [44,60] that are expressed in Caco-2 cells and capable of modulating cell proliferation.

We have first investigated the potential implication of PKCα in cytostatic and morphologic effects of huratoxin and epoxy-huratoxin using its pharmacological inhibitor Gö6976 (Fig. 10). As shown in Figs. 10A and 10B, the inhibition of PKCα did not change the growth inhibition and the cell aggregation induced by both compounds. Even though not significative, in basal conditions a Caco-2 cell growth increase was repeatedly measured upon

PKCα inhibitor incubation (Fig. 10A). This suggests that PKCα could play a cytostatic role in basal conditions as previously reported [56]. Moreover, the expression of PKCα was strongly decreased after huratoxin and epoxy-huratoxin treatment (Fig. 10B). This strong decrease of PKCα expression could be related to the previous work of Rickard and coll.[61] showing that short-chain fatty acids incubated with Caco-2 cells induce a specific down-regulation of PKCα. Rickard *et al.* demonstrate that this reduced expression of PKCα is not secondary to its enzymatic activation or to cell differentiation. Their data suggest that a degradation of the enzyme occurs independently from metabolic changes but under the control of gene transcription. Interestingly, the authors propose that the downregulation of PKCα should be a mechanism supporting the antitumorigenic action of specific short-chain fatty acids such as butyrate. Thus, this mechanism could reinforce the recovery of normal tissue functions induced by mono-esterified daphnanes. On the other hand, eventhough the treatment by the PKCα inhibitor has increased the expression of PKCδ, its active form (pSer664 PKCδ) is absent upon treatment with huratoxin with or without PKCα inhibitor (Fig. 10C). Altogether, these data show that conventional and novel PKCs seem not to be implicated in the activity of huratoxin and its epoxide derivative.

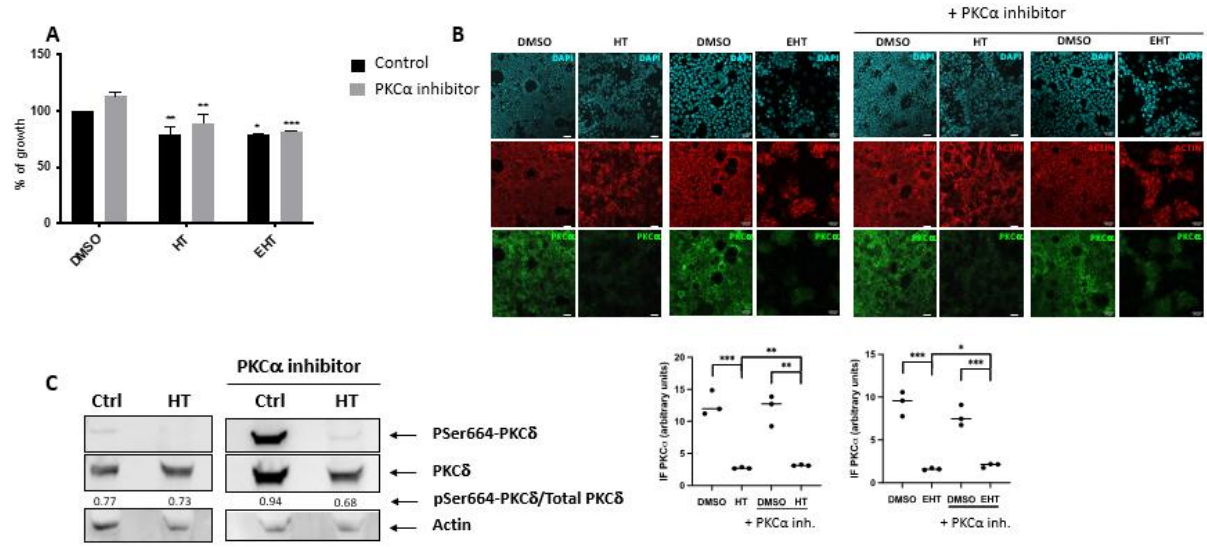

*Figure 10: Regulation of PKCα and PKCδ under treatment of Caco-2 cells by huratoxin and 4',5'-epoxy-huratoxin. Caco-2 cells were pretreated for 15 min with 0.2 µM PKCα inhibitor (Gö6976) and then incubated with huratoxin (HT) and epoxy-huratoxin (EHT) at 1 µg/mL. A) After 48 h of incubation, cell viability was measured by colorimetry and the activity of huratoxin and epoxy-huratoxin was calculated relative to the DMSO control (Caco-2 cells treated with DMSO solvent only). Mean ± S.E.M. from 1 to 3 (n) independent experiments in triplicates and statistical 2 ways ANOVA test compared to DMSO controls in the presence or absence of PKC inhibitor: *p<0.05, **p<0.01, ***p<0.001. B) Morphological impact of huratoxin and epoxy-huratoxin treatment in the presence or not of PKCα inhibitor. After 48 h of incubation, PKCα immunostaining was performed (green) and quantified by immunofluorescence (graphs, statistical t-test, *p<0.05, **p<0.01, ***p<0.001). Labeling of nuclei (cyan) and cytoskeleton (red) is shown. Confocal views, 20X objective, size scale= 50 µm, representative of duplicate from one experiment. C) After 48 h of incubation, cells were lysed for Western blot analysis. The results obtained from the revelation of the phosphorylated form (pSer664) and the total form of PKCδ are shown as well as quantification of pSer664-PKCδ/Total PKCδ. Actin shows the equivalence of protein deposition. Ctrl=Control DMSO. Data are from one experiment.*

Then we decided to investigate the involvement of atypical PKCs (aPKCs ζ and ι) in the cytostatic and morphological activities of daphnanes. Caco-2 cells were incubated with an aPKCs inhibitor (CRT0066854 hydrochloride) for 30 minutes before treatment with huratoxin or epoxy-huratoxin at 1 µg/mL. This aPKCs inhibitor binds to the ATP-binding site of the enzyme and to a nearby residue to induce the inactive conformation of the kinase [62]. As shown in Fig.11A, the presence of the aPKCs inhibitor dramatically reduced the inhibition of cell growth induced by the two daphnanes whose difference in effect with the control has become statistically non-significant. Similarly, the presence of this aPKCs inhibitor implied a lack of morphological changes on Caco-2 cells induced by epoxy-huratoxin and huratoxin as illustrated in Fig. 11B. Indeed, through labeling of the Caco-2 cytoskeleton and nuclei (Fig. 11B), we show that actin is more compacted and cells more aggregated upon huratoxin treatment compared to 4',5'-epoxy-huratoxin. Furthermore, the inhibition of PKCζ decreased actin density and cell aggregation in huratoxin and 4',5'-epoxy-huratoxin assays, respectively. These observations suggest that the targets of activated PKCζ upon treatments with huratoxin and 4',5'-epoxy-huratoxin could be primarily actin reorganization and cell-cell adhesive contacts, respectively. Moreover, we were able to establish that the impact of CRT0066854 hydrochloride on the inhibition of cytostatic effects of the two daphnanes was dose-dependent (data not shown), and to determine the dose 1.25 µM for which 50% of the effect of the daphnanes is inhibited. It has been shown by Xiong and colleagues that, compared with the ι-isoform, the ζ-isoform of aPKCs played a prominent role in the morphogenesis of Caco-2 cells [63]. Consequently, our results strongly suggest the involvement of PKCζ in the cytostatic and adhesive effects of the tested orthoesterified daphnanes. Thus, we studied the effect of huratoxin and epoxy-huratoxin on the activation state of PKCζ. As shown in Fig. 11C, the phosphorylation of Threonine 410 of PKCζ is increased only upon treatment with huratoxin. This threonine is localized to the kinase activation loop and its phosphorylation raises the activity of the kinase but is not absolutely essential to it [64,65].

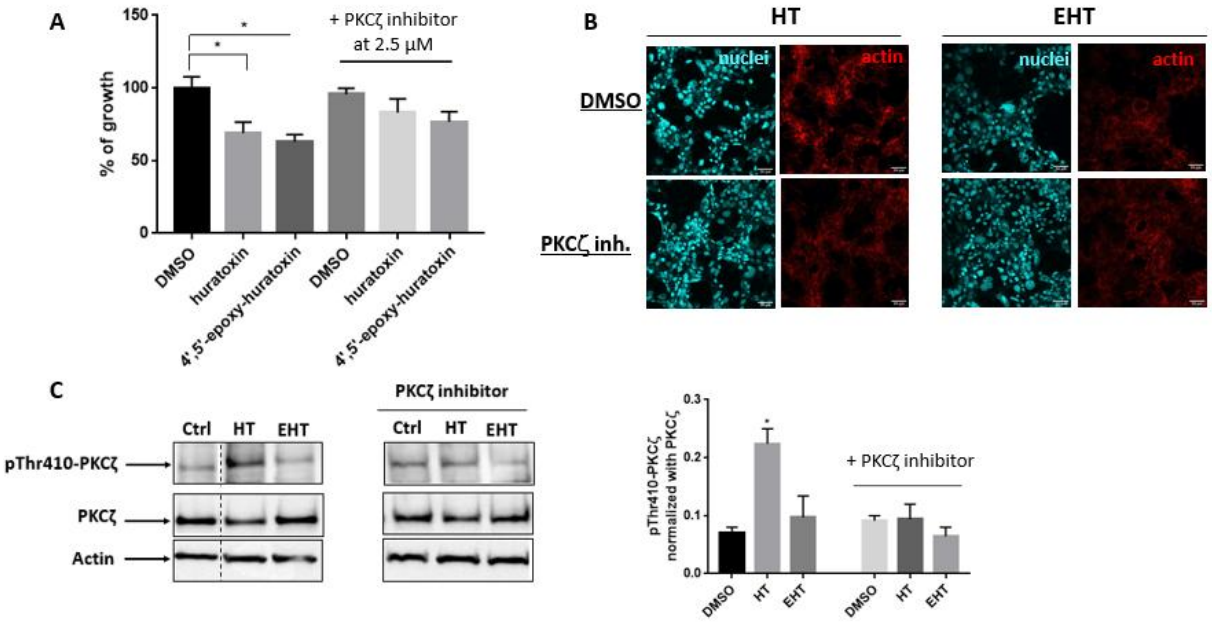

*Figure 11: Involvement of PKCζ in the cytostatic and morphological activities of huratoxin and 4',5'-epoxy-huratoxin. Caco-2 cells were pretreated for 30 min with 2.5 µM PKCζ inhibitor (CRT0066854 hydrochloride) and then incubated with daphnanes at 1 µg/mL. A) After 48 h of incubation, cell viability was measured by colorimetry and the activity of daphnanes was calculated relative to the DMSO control (Caco-2 cells treated with DMSO solvent only). Mean ± S.E.M. from 3 (n) independent experiments and t-test compared to DMSO controls in the presence or absence of PKCζ inhibitor: *p<0.05. B) Morphological impact of Caco-2 cells pretreatment with the PKCζ inhibitor before addition of huratoxin (HT) or 4',5'-epoxy-huratoxin (EHT). Nuclei (cyan) and cytoskeleton (red) labeling (confocal views taken at the OPERA Phenix®, 20X objective, size scale = 50 µm). Photographs are representative of duplicates from one experiment. C) After 48 h of incubation cells were lysed for Western blot analysis. The results obtained from the revelation of the phosphorylated form (pThr410) and the total form of PKCζ are shown. Actin shows the equivalence of protein deposition. The modulation of the phosphorylated active form of PKCζ (pThr410) after addition of the PKCζ inhibitor is shown. Quantification of n=2 experiments and statistical t-test compared to DMSO are shown : Mean ± S.E.M., *p<0.05.*

To further understand the mechanism of action of daphnanes, we examined the localization of PKCζ after treatment with huratoxin and epoxy-huratoxin at 1 µg/mL. As depicted in Fig. 12A, upon treatment with both daphnanes, the co-localization of PKCζ and actin is increased compared to the control. Moreover, upon treatment with huratoxin, PKCζ was found co-localized with actin in dense cell aggregates whereas this co-localization was found more peripheral to cell aggregates upon treatment with 4',5'-epoxy-huratoxin (Fig. 12B and 12C). Of note, PKCz was rarely found in the nucleus of Caco-2 cells treated with both daphnanes. Involvement of PKCζ in the polarity complex PKCζ-Par3-Par6-cdc42 (PKCζ-Partitioning defective protein 3- Partitioning defective protein 6- Cell division control protein 42) [21,25,27] may explain the reorganization of Caco-2 cells interactions after PKCζ activation. Thus, both huratoxin and epoxy-huratoxin would be able to activate PKCζ and induce its relocalization but by different mechanisms. The underlying action of epoxy-huratoxin on PKCζ needs to be investigated.

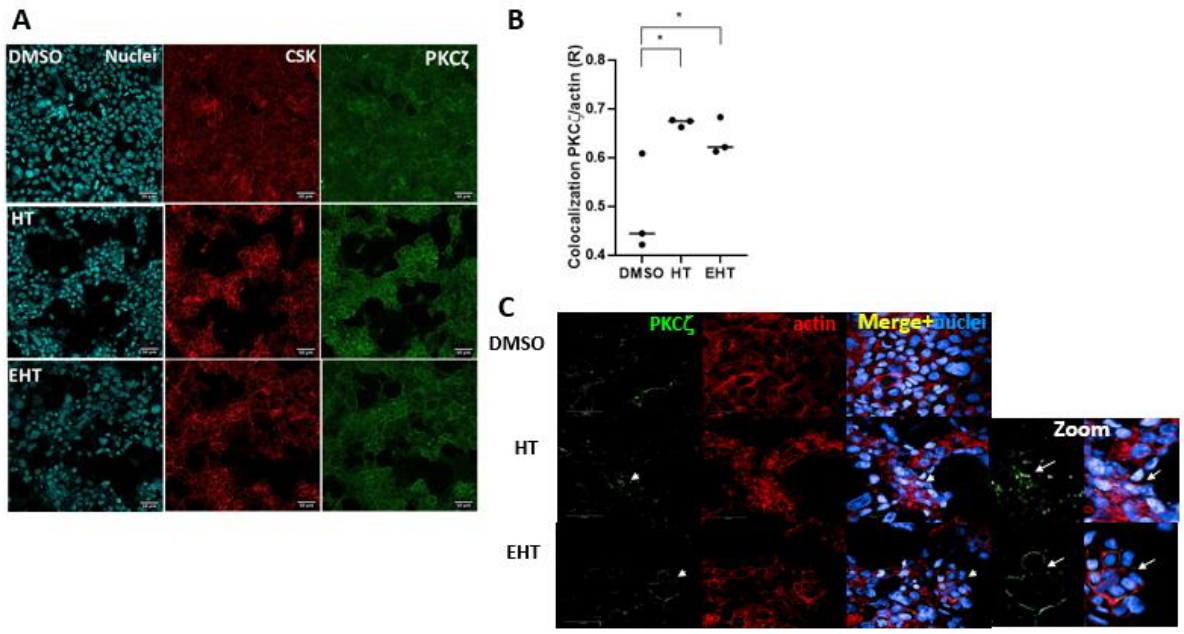

*Figure 12: Effects of huratoxin and epoxy-huratoxin on PKCζ localization. Caco-2 cells were incubated with huratoxin (HT) and epoxy-huratoxin (EHT) at 1 µg/mL for 48 h and PKCζ immunostaining was performed (green). Labeling of nuclei (cyan in A, blue in B) and actin (CSK, red) is shown. Confocal views were taken at the OPERA Phenix® (A, 20X objective; B, 63X objective; size scale = 50 µm; representative of duplicates from one experiment. Zoom of critical zones are shown on the right in B. In A, a quantification of the colocalization of actin and PKCζ is shown (statistical t-test, *p<0.05).*

2.5. Impact of huratoxin and epoxy-huratoxin on adhesive and proliferative signaling pathways

As previously shown by our team [50], huratoxin induces inhibition of GSK3β and Akt kinases (Fig. 13), which are major signals controlling cancer cell proliferation and adhesion [66,67]. This is not surprising, considering that in response to a hyperproliferative stimulus in the colonic epithelium, a strong association between PKCζ and GSK3β occurs and is associated with phosphorylation on serine 9 of GSK3β, signaling its inactivation [68]. As shown in Fig.13, treatment with epoxy-huratoxin increases the inactive form of GSK3β (pSer9-GSK3β) and abolishes the active form of Akt (pSer473-Akt), thus both daphnanes have the same mechanism of action on these signaling pathways. Nevertheless, it can be observed an important increase of Akt expression after treatment by both compounds suggesting changes in the proteasomal degradation of Akt [69]. Of note, expression of the potential target of GSK3β and Akt, β catenin, playing a critical role in both adhesion and proliferation of epithelial progenitors, is not modified after treatment by daphnanes (Fig. 13). Additionally, Fig.13 shows that prior incubation of cells with PKCζ inhibitor abrogates the increase in pSer9

GSK3β upon treatment with orthoesterified daphnanes, suggesting that activation of PKCζ by these compounds is required for GSK3β inhibition.

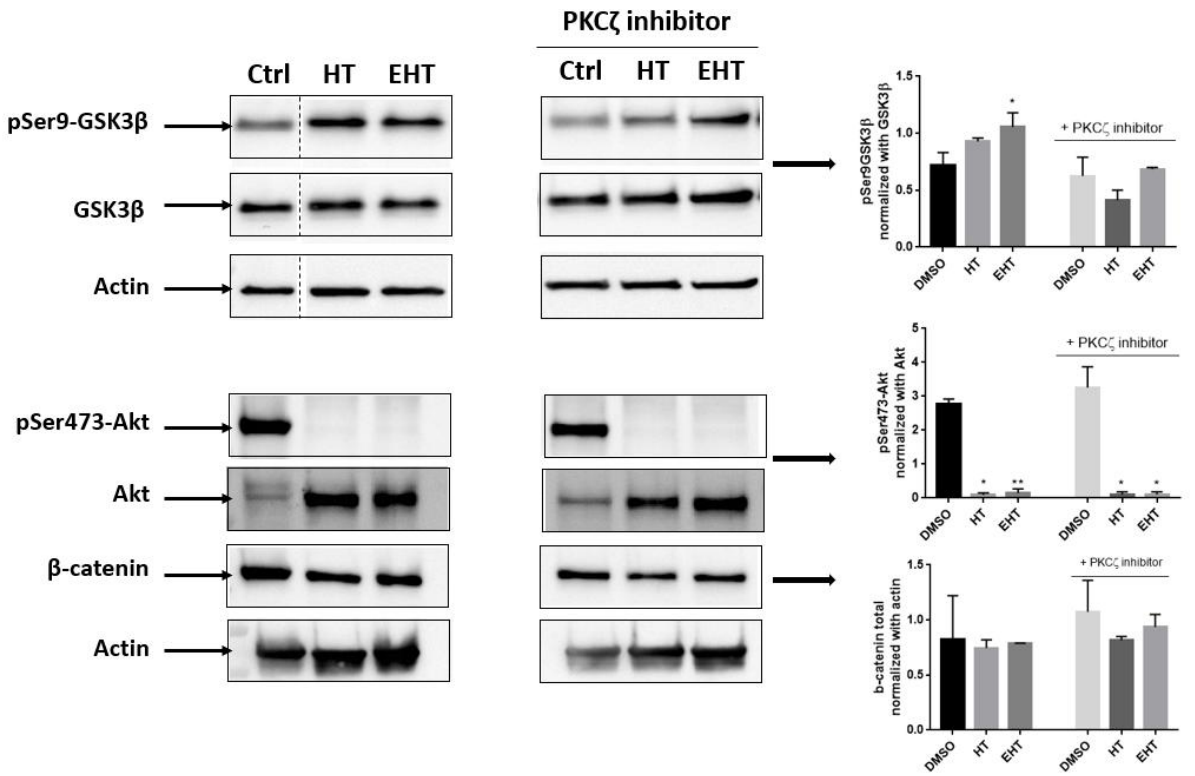

*Figure 13: Regulation of GSK3β, Akt and β-catenin by huratoxin and 4',5'-epoxy-huratoxin. Caco-2 cells were pretreated or not for 30 min with 2.5 µM PKCζ inhibitor (CRT0066854 hydrochloride) prior to huratoxin (HT) or 4',5'-epoxy-huratoxin (EHT) treatment (1 µg/mL). After 48 h of incubation, cells were lysed for Western blot analysis. The results obtained from the revelation of the phosphorylated forms (pSer9-GSK3β; p-Ser473-Akt) and the total forms of GSK3β, Akt and β-catenin are shown. Actin shows the equivalence of protein deposition. Quantification of n=2 experiments and statistical t-test compared to DMSO (Ctrl) are shown: Mean ± S.E.M., *p<0.05, **p<0.01.*

A direct phosphorylation of GSK3β on serine 9 by PKCζ has not be documented so far. To further characterize the underlying mechanism of GSK3β inhibition by the tested daphnanes, we studied other GSK3β partner signaling pathways such as MEK which may be involved in PKCζ-dependent regulation of GSK3β. Indeed, MEK can phosphorylate serine 9 of GSK3β and can be activated by PKCζ [70,71]. As depicted in Fig.14A, pharmacological inhibition of MEK abolishes the cytostatic effect of huratoxin, confirming its implication. However, its status of activation (pSer217/221-MEK) is unchanged upon treatment with daphnanes, whereas it is increased when Caco-2 cells are pre-treated with the PKCζ inhibitor (Fig. 14B). Given our previous work [50] showing that huratoxin does not activate the kinase Erk which is downstream of MEK in the signaling pathway triggered by activated membrane receptors, these results suggest that MEK may play a specific role in a tripartite

PKCζ/MEK/GSK3β complex, proximal to the plasma membrane and responsible for the phosphorylation of GSK3β under treatment by huratoxin or epoxy-huratoxin.

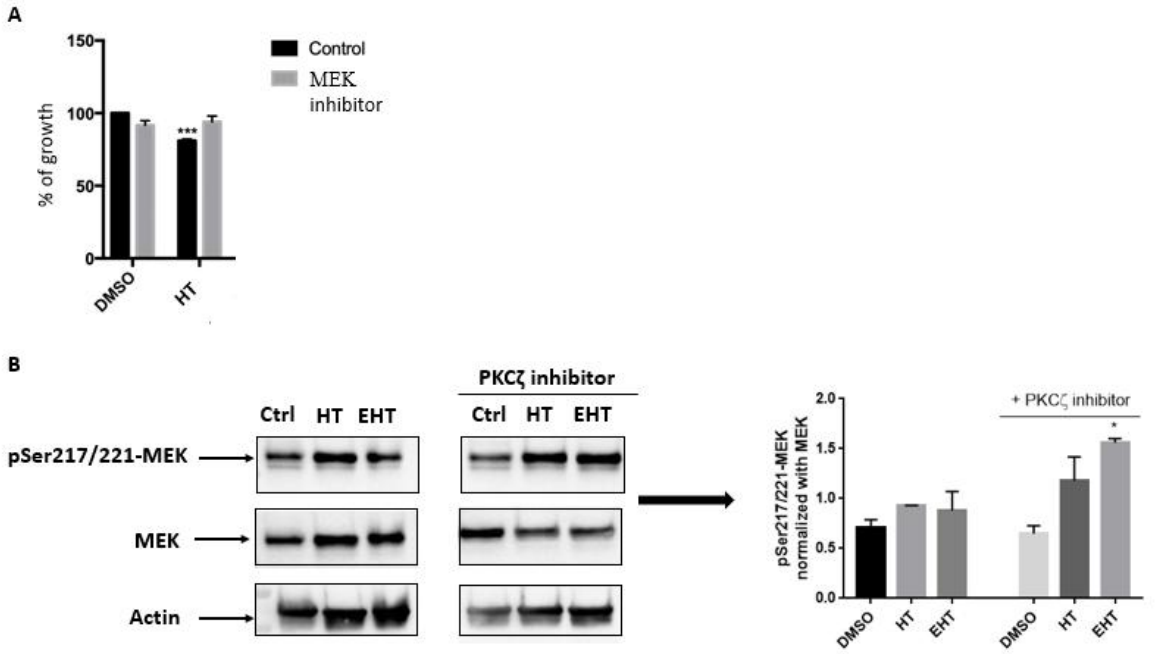

*Figure 14: Implication of MEK in the cytostatic effects of mono-esterified daphnanes. A) Huratoxin (1 µg/mL) was incubated with Caco-2 cells for 48 h before cell viability test. Prior addition of huratoxin, a MEK inhibitor (PD0325901) was added or not for 15 min at the concentration of 0.5 µM. Data are from n=3 experiments, Mean ± S.E.M., statistical t-test compared to DMSO (Ctrl) are shown: ***p<0.001. B) Huratoxin (HT) and 4',5'-epoxy-huratoxin (EHT) at 1 µg/mL were incubated with Caco-2 cells which have been pretreated or not for 30 min with 2.5 µM PKCζ inhibitor (CRT0066854 hydrochloride). After 48 h of incubation, cells were lysed for Western blot analysis. The results obtained from the revelation of the phosphorylated form (pSer217/221-MEK) and the total form of MEK are shown. Actin shows the equivalence of protein deposition. Quantification of n=2 experiments and statistical t-test compared to DMSO(Ctrl) are shown: Mean ± S.E.M., *p<0.05.*

Besides, it has been reported that various diterpenes possess antiviral properties [9,10,13–18,20,72] and that the activation of PKCs in host cells is implied in the mechanism of action of those diterpenes [19,32]. In other hand, it has also been described that phosphorylation of the SARS-CoV-2 nucleocapsid (N) protein by the GSK3 kinase is required for viral interaction with host cells, as well as for viral transcription and replication [73,74]. In this study, we show that huratoxin and 4',5'-epoxy-huratoxin induce the inhibition of GSK3 kinase, thus we speculate that the present daphnane diterpenes may be of interest in fighting SARS-CoV-2 and/or Zika viruses. A sampling of isolated diterpenes (compounds **5**, **6** and **7**) has therefore been assessed against SARS-CoV-2 and ZIKV. Unfortunately, the three derivatives were inactive against ZIKV (IC_{50} > 50 µM) and were not able to reduce SARS-CoV-2 progeny production at non-cytotoxic concentrations (IC_{50} 34.2, 64.2 and 50.2 µM for **5**, **6** and **7**, respectively).

2.6. Cytostatic tests on human primary cells

To evaluate the cytostatic activity of orthoesterified daphnanes *ex vivo*, huratoxin and epoxy-huratoxin were tested on human primary cells cultured as colonoids. Indeed, it is considered that colonoids derived from patients' primary cells have the same characteristics as *in vivo* tumor, allowing a pre-clinical evaluation [75]. As shown in Fig. 15A, at 1 µg/mL, huratoxin and epoxy-huratoxin present a cytostatic effect on all organoids (control (1,2,3) and CRC (4,5)) but overall, more pronounced on cancerous organoids. Interestingly, at the same concentration, the antimetabolite cytostatic agent 5-fluoro-2'-deoxyuridine (5FdU), used in the treatment of metastatic colorectal cancer in USA [76], has no effect on all organoids as depicted in Fig. 15A. ~~The Figure 14B shows that daphnanes induce a decrease in colonic organoid size without evidence of cell death.~~ Thus, the present patient samples seem to be resistant to 5FdU while huratoxin and epoxy-huratoxin keep their cytostatic activity. The dose dependent effects illustrated in Fig. 15B, revealed that, at 0.1 µg/mL, huratoxin and epoxy-huratoxin have a selective cytostatic activity on CRC organoids with 40% of growth inhibition. These results suggest that huratoxin and 4'-5'-epoxy-huratoxin may be good candidates for *in vivo* antitumor evaluations.

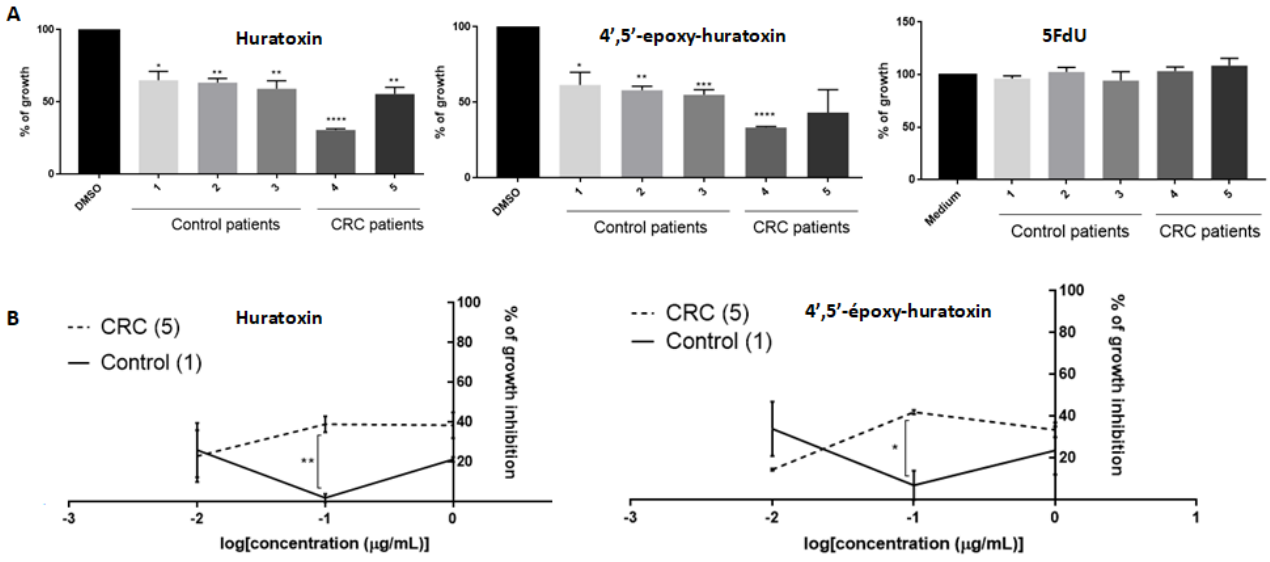

*Figure 15: Cytostatic activity of huratoxin and 4',5'-epoxy-huratoxin on 3D cultures of human primary colorectal cells. Colorectal epithelial cells were isolated from control (1, 2, 3) and CRC patients (4,5) and cultured as organoids ex vivo. After 48 h of organoid formation from individual cells, incubation with huratoxin, epoxy-huratoxin, 5FdU or DMSO (Control) for 48 h was performed. Then cell viability was measured by luminescence and cytostatic activity was calculated compared to the control (DMSO or medium). A) Compounds were incubated at 1 µg/mL. Mean ± S.E.M. from triplicates (patients 1-4) or duplicates (patient 5) of 1 (patients 2, 4) or 2 (patients 1, 3, 5) independent experiments and statistical t-test compared to control (DMSO, medium) are shown: *p<0.05, ** p<0.01, ***p<0.001, ****p<0.0001. B) Organoids from patient 1 (Control) and patient 5 (CRC) were incubated with huratoxin or 4',5'-epoxy-huratoxin at 0.01, 0.1 or 1 µg/mL or DMSO and cell viability was measured as in A. Cytostatic activities were calculated compared to control DMSO. Mean ± S.E.M. from 1 (n) experiment and statistical t-test compared to control are shown: *p<0.05, **p<0.01.*

2.8. Conclusions

Five new daphnane-type diterpenes named 6'*R*-hydoxy-huratoxin, 4'*S*,5'*S*-dihydroxy-huratoxin, 4'(*Z*)-6'-oxo-huratoxin, 4'*S*,5'*S*-epoxy-huratoxin and huratoxigenin-20-(11'-methyloctadec-12'-enoate), along with two known daphnanes (huratoxin and 6'-oxo-huratoxin) were isolated with several separative techniques from the latex of *H. crepitans* and their structures were elucidated by different spectroscopic methods. Their biological assessment on Caco-2 cells highlighted huratoxin and 4',5'-epoxy-huratoxin as the most interesting compounds while C-20 ester **5** was inactive. This pointed that orthoesterified side chain is required for anti-proliferative activity and epoxy substitution can exalt this activity. The anti-proliferative effect of huratoxin and epoxy-huratoxin appeared to be dependent on the atypical PKCζ. Furthermore, both compounds can induce relocation of the kinase at the plasma membrane, whereas only huratoxin leads to an increase of one of the active forms of PKCζ. Thus, these two derivatives activate PKCζ but by two different ways and the mechanism by which epoxy-huratoxin stimulates PKCζ is yet unresolved. More precisely, both orthoesterified daphnanes were able to inhibit Akt and GSK3β, that are two major signaling pathways implicated in tumoral cell proliferation and survival. Our results suggest that inhibition of PKCζ abolishes GSK3β inhibition whereas Akt inhibition is unchanged, and induces an increase in MEK activation after treatment with huratoxin and epoxy-huratoxin. It also can be added that a tripartite PKCζ/MEK/GSK3β complex could be formed at a proximal site of the plasma membrane at the expense of other membrane receptors, which could trigger GSK3β inhibition. Finally, evaluation of the cytostatic activity of the two orthoesterified daphnanes on *ex vivo* primary human cells cultured as colonoids revealed that they selectively inhibited cancer cells growth from 0.1 µg/mL making them good candidates for *in vivo* antitumor evaluations.

3. Materials and methods

3.1. Chemistry

3.1.1. Plant material

The latex of *H. crepitans* L. was collected in the area of Mazan, Peru (3°30'04.0''S/73°05'12.5W), in June 2019 by Dr Billy Joel Cabanillas. A herbarium board

(N° Hc2019-1) was deposited in the herbal collection of the faculty of pharmaceutical sciences of Toulouse (France).

3.1.2. Analytical chemistry material

Circular dichroism spectra were measured on a JASCO J-815 spectrometer, controlled by Spectra Manager software. UV spectra were acquired on a Jasco J-815 UV–visible spectrophotometer and IR spectra were measured on a Fourier transform spectrophotometer FRONTIER FT-IR (PerkinElmer) controlled by Spectrum software. Optical rotation was measured on a JASCO P-2000 polarimeter.

Compounds were isolated using a BUCHI MPLC system equipped with two pumps C-0605 and controlled by a C-615 pump manager (BUCHI). Borosilicated glass columns were conditioned by silica gel Kieselgel 60 (MACHEREY-NAGEL) previously activated at 100°C for 24 h. Column chromatographies were performed using borosilicated glass columns conditioned by silica gel Kieselgel 60 (MACHEREY-NAGEL) previously activated at 100°C for 24 h or silica LiChroprep RP-18 gel (MACHEREY-NAGEL). PuriFlash system (XS520Plus, Interchim) was used with RS 80 C18 column or RS 15 C18 column (CHROMABOND Flash, MACHERY-NAGEL). Semi preparative HPLC was performed with a HITACHI LaChrom system (MERCK) consisting in a quaternary LaChrom L-7100 pump and a LaChrom L-7455 photodiode array detector, using a Luna column C18 100 Å (10 X 250 mm, 5 µm) (Phenomenex). UHPLC/DAD/HRMS analyzes were performed using an UHPLC Ultimate 3000 system (Dionex) equipped with LTQ-Orbitrap XL mass spectrometer (Thermo Fisher Scientific), a Diode Array Detector system (Dionex) and a Waters Acquity C18 UPLC BEH 100 Å column (2,1 x 150 mm, 1,7 µm). Chromeleon Xpress 6.8 (Dionex) and Xcalibur 3.0 (Thermo Fischer Scientific) software were used for data acquisition and analysis. Samples were centrifugated with a centrifuge 5804 R (Eppendorf). NMR spectra were acquired on a Bruker AVANCE 300 and a Bruker AVANCE 500 spectrometer equipped with a 5 mm TCI Prodigy CryoProbe using TMS as reference. Spectrometers were controlled with Topspin software and spectra were analyzed with NMR MNova software.

3.1.3. Extraction and isolation of daphnane diterpenes

3.1.3.1. Extraction of the latex of H. crepitans

Notches in the trunk of several trees were made to collect the latex of *H. crepitans*. Then, the lyophilisated latex (1250 g) was extracted twice with 2 x 12.5 L of boiling CH_2Cl_2

during 3 h 30 with stirring. After two successive paper filtrations, the residue was extracted with 12.5 L of EtOH 96% during 24 h with stirring. Therefore, 3 extracts were obtained: CH_2Cl_2 n°1 (42.53 g), CH_2Cl_2 n°2 (6.15 g) and ethanolic extract (36.35 g).

3.1.3.2. Precipitation of cerebrosides

The CH_2Cl_2 n°1 crude extract was dissolved in 350 mL of cyclohexane and centrifuged at 3000 rpm for 20 min. The supernatant was recovered and the precipitate was washed 3 times with cyclohexane. The precipitate labeled as fraction EC.2.21.A (4.1529 g). The washing solvent was combined with the supernatant to obtain the fraction EC.2.21.B (38.3203 g).

3.1.3.3. Fatty acids elimination

The first daphnanes fractionation and isolation assays were affected by the high content of fatty acids in the latex, particularly palmitic acid ($C_{16}H_{32}O_2$). It was therefore decided to discard them by liquid/liquid extraction. The fraction EC.2.21.B was dissolved in a biphasic system consisting in a mixture of cyclohexane (4 L)/isopropanol (4 L)/distilled water containing 20 mM of triethylamine (4 L). After agitation and cooling, aqueous and organic phases were dried to give fractions EC.2.23.A (12.30 g) and EC.2.23.B (25.99 g), respectively. Thanks to triethylamine, the fatty acids are in ionized form and soluble into the aqueous phase (mixture of water and isopropanol), whereas the daphnanes remain in the organic phase (mixture of cyclohexane and isopropanol).

3.1.3.4. Fractionation of the defatted extract by Medium Pressure Liquid Chromatography (MPLC)

MPLC separations were performed on silica gel at a flow of 40 mL/min and fractions were controlled for their content by UHPLC-(+)APCI-MS according to the method described by Trinel *et al.* [8]. The fraction EC.2.23.B was chromatographed using cyclohexane (500 mL), cyclohexane/CH_2Cl_2 50/50 (v/v) (750 mL), CH_2Cl_2 (500 mL), CH_2Cl_2/EtOAc 50/50 (v/v) (750 mL), EtOAc (750 mL), EtOAc/MeOH 50/50 (v/v) (750 mL) and MeOH (500 mL). This fractionation was repeated 3 times with 8.7 g of EC.2.23.B. Fractions were pooled to give five subfractions (EC.2.30.A to EC.2.30.E). Fractions EC.2.30.C (0.9555 g) and EC.2.30.D (4.2135 g) were found to be enriched in mono-esterified daphnanes. Fraction EC.2.30.B consisted in a mixture of mono- and diesterified daphnanes, whereas fraction EC.2.30.E was composed of mono-esterified daphnanes and cerebrosides. Fraction EC.2.30.B (2.9904 g) was

chromatographed with CH_2Cl_2 (1 L), CH_2Cl_2/EtOAc 80/20 (v/v) (750 mL), CH_2Cl_2/EtOAc 50/50 (v/v) (750 mL), EtOAc (500 mL) and MeOH (750 mL). Fractions were pooled according to their UHPLC-MS profiles to give 4 subfractions (EC.2.32.A to EC.2.32.D), all containing mono-esterified daphnanes. Fraction EC.2.30.E (8.7650 g) was chromatographed with CH_2Cl_2 (500 mL), CH_2Cl_2/EtOAc 50/50 (v/v) (500 mL), EtOAc (500 mL), EtOAc/MeOH 90/10 (v/v) (500 mL), EtOAc/MeOH 70/30 (v/v) (500 mL), EtOAc/MeOH 50/50 (v/v) (500 mL) and MeOH (500 mL) leading to 4 subfractions (EC.2.34.A to EC.2.34.D). Fractions EC.2.34.B (1.5982 g) and EC.2.34.C (2.1476 g) contained mono-esterified daphnanes. Finally, fractions EC.2.34.C and EC.2.30.D were pooled in fraction EC.2.42.B (6.3611 g).

3.1.3.5. Isolation of mono-esterified daphnanes

Fraction EC.2.32.C (0.5987 g) was fractionated on silica gel column with cyclohexane (250 mL), CH_2Cl_2 (150 mL), EtOAc (240 mL) and MeOH (200 mL) to give 3 subfractions (EC.2.36.A to EC.2.36.C). Fraction EC.2.36.B (0.4805 g) was separated on the same column with CH_2Cl_2/EtOAc 50/50 (v/v) (180 mL), CH_2Cl_2/EtOAc 40/60 (v/v) (340 mL) and EtOAc (150 mL), leading to 8 fractions (EC.2.40.A to EC.2.40.H). Fractions EC.2.40.G and EC.2.40.H (0,0187 g) were grouped with fraction EC.2.30.C to form fraction EC.2.41.C (0.9381 g). Fraction EC.2.41.C was partitioned by MPLC on a 80 g (RS 80) C18 column using a H_2O (A)/MeCN (B) gradient at a flow rate of 60 mL/min. Twelve fractions were collected (EC.2.43.A to EC.2.43.L) using a linear gradient (from 50 to 100% of B in 60 min). Fraction EC.2.43.I (0.0748 g) was chromatographed by semi preparative HPLC using a distilled water (A)/MeCN (B) gradient consisting in 99% B from 0 to 10 min, 99-100% B from 10 to 11 min and 100% B from 11 to 20 min and leading to huratoxin (compound **6**, 30.17 mg) and huratoxigenin-20-(11'-methyloctadec-12'-enoate) (compound **5**, 4.37 mg).

Fraction EC.2.43.F (0.0796 g) was treated by semi preparative HPLC (80 to 100% B from 0 to 20 min and 100% B from 20 to 30 min) and gave pure 6'-oxo-huratoxin (compound **7**, 37.47 mg) and 4'(*Z*)-6'-oxo-huratoxin (compound **3**, 6,02 mg). Fraction EC.2.42.B (6.3611 g) was partitioned by 4 successive MPLC following the same gradient than for fraction EC.2.41.C to give 7 fractions (EC.2.65.A to EC.2.65.G). Fraction EC.2.65.E (0.1115 g) was treated by semi preparative HPLC (0-30 min: 70 to 100% B, 30-40 min: 100% B) to give 6'-hydroxy-huratoxin (compound **1**, 8.33 mg). Fraction EC.2.65.C (0.0802 mg) was partitioned by MPLC with linear gradient (from 30 to 70% B in 60 min) at a flow rate of 20 mL/min and gave 10 fractions (EC.2.90.A to EC.2.90.J). Fraction EC.2.90.J (0.0121 g) was

treated by semi preparative HPLC (0-25 min: 65% of B, 25-25.1 min 65-100% B, 25.1-35 min: 100% B) leading to 4',5'-dihydroxy-huratoxin (compound **2**, 1.32 mg). Fraction EC.2.65.G (0.2652 g) was separated by MPLC (from 40 to 80% B in 60 min) at a flow rate of 20 mL/min to give 7 fractions (EC.2.103.A to EC.2.103.G). Fraction EC.2.103.G (0.0575 g) was treated by semi preparative HPLC (0-20 min: 90%, 20-20.1 min: 100% B, 20,1-30 min: 100% B) leading to 3 fractions (EC.2.107.A to EC.2.107.C). EC.107.C (0.0037 g) was purified by semi preparative HPLC following the same gradient and gave 4',5'-epoxy-huratoxin (compound **4**, 2.32 mg).

6'*R*-hydroxy-huratoxin **1:** colorless oil, $[\alpha]_{25}^{D}$ +28.49 (c 0.463; CH_2Cl_2); IR υ_{max} 3446, 2924, 2855, 1697, 1038, 997 cm^{-1}; ^{1}H and ^{13}C NMR data (CD_2Cl_2, 500 MHz), see Table 1; HRAPCIMS *m/z* 601.3362 $[M+H]^+$ Δppm = -1.546 (calcd for $C_{34}H_{49}O_9^+$, 601.3377).

4'*S*,5'*S*-dihydroxy-huratoxin **2:** colorless oil, $[\alpha]_{25}^{D}$ +26.71 (c 0.073; CH_2Cl_2); IR υ_{max} 3384, 2924, 2855, 1701, 1073, 1034, 974 cm^{-1}; ^{1}H and ^{13}C NMR data (CD_2Cl_2, 500 MHz), see Table 1; HRAPCIMS *m/z* 619.3476 $[M+H]^+$ Δppm = -0.120 (calcd for $C_{34}H_{51}O_{10}^+$, 619.3482).

4'(*Z*)-6'-oxo-huratoxin **3:** colorless oil, $[\alpha]_{25}^{D}$ +30.12 (c 0.334; CH_2Cl_2); IR υ_{max} 3462, 2925, 2856, 1694, 1034, 995 cm^{-1}; ^{1}H and ^{13}C NMR data (CD_2Cl_2, 500 MHz), see Table 1; HRAPCIMS *m/z* 599.3206 $[M+H]^+$ Δppm = -1.501 (calcd for $C_{34}H_{47}O_9^+$, 599.3220).

4'*S*,5'*S*-epoxy-huratoxin **4**: colorless oil; $[\alpha]_{25}^{D}$ + 19.38 (c 0.129; CH_2Cl_2); IR υ_{max} 3421, 2924, 2855, 1701, 1074, 1034, 966 cm^{-1}; ^{1}H and ^{13}C NMR data (CD_2Cl_2, 500 MHz), see supporting information; HRAPCIMS *m/z* 601.3367 $[M+H]^+$ Δppm = -0.731 (calcd for $C_{34}H_{49}O_9^+$, 601.3377).

Huratoxigenin-20-(11'-methyloctadec-12'-enoate) **5:** colorless oil, $[\alpha]_{25}^{D}$ -21.98 (c 0.243; CH_2Cl_2); IR υ_{max} 3420, 2924, 2855, 1707, 1054 cm^{-1}; ^{1}H and ^{13}C NMR data (CD_2Cl_2, 500 MHz), see Table 1; HRAPCIMS *m/z* 675.4459 $[M+H]^+$ Δppm = -1.184 (calcd for $C_{39}H_{63}O_9^+$, 675.4472).

Huratoxin **6**: colorless oil; ^{1}H NMR data (CD_2Cl_2, 300 MHz), see supporting information; HRAPCIMS *m/z* 585.3422 $[M+H]^+$ Δppm = 0.043 (calcd for $C_{34}H_{49}O_8^+$, 585.3427).

6'-oxo-huratoxin **7:** colorless oil; ^{1}H and ^{13}C NMR data (CD_2Cl_2, 500 MHz), see supporting information; HRAPCIMS *m/z* 599.3204 $[M+H]^+$ Δppm = -1.718 (calcd for $C_{34}H_{47}O_9^+$, 599.3220).

3.1.4. Computational details for GIAO NMR chemical shifts calculations

All *ab initio* calculations were performed using the Gaussian 09.D01 program (Ref). The different stereoisomers of each compound studied were first subjected to a conformational search using the MMFF94 force-field implemented in TINKER software tools, resulting in 25 to 30 conformers for each stereoisomer [77]. The resulting conformations were then subjected to further optimization at the B3LYP/6-31G* level of theory. The bulk solvent effects were described with the integral equation formalism polarizable continuum Model (IEFPCM) with dichloromethane as solvent [78]. The vibrational frequencies were computed in order to access the free energies and to confirm the absence of imaginary frequencies. The magnetic shielding constants (σ) were computed using the gauge-including atomic orbitals (GIAO) [79,80] method at the MPW1PW91/6-31+G** level of theory. The resulting shielding tensors of the set of conformers were averaged by computing the Boltzmann-weighted population [81]. The chemical shifts were calculated from TMS as reference standard. The systematic errors were removed by scaling according to $\delta_{scaled} = (\delta_{calc} - Intercept)/Slope$, where Intercept and Slope, result from a linear regression calculation on a plot of δ_{calc} against δ_{exp} [79]. The DP4+ probabilities were then computed as originally described by Smith and Goodman [51] and Grimblat *et al* [82].

3.2. Biological

3.2.1. Evaluation of the antiproliferative activity of isolated mono-esterified daphnanes

3.2.1.1. Cell cultures

The human colon adenocarcinoma cell line Caco-2 (HTB-37™) was purchased from the American Type Culture Collection (ATCC). This cell line has the *Adenomatous Polyposis Coli* (APC) gene mutated like in 80% of CRC. Caco-2 cells were cultured in DMEM medium with 4.5 g/L of glucose, 1% GlutaMAX and 1% pyruvate (GIBCO, 31966) supplemented with 10% SVF (GIBCO), 1% non-essential amino acids (GIBCO) and 1% penicillin and streptomycin mixture (P/S, GIBCO). The human small intestine cell line HIEC6 was purchased from ATCC (CRL-3266™). HIEC6 cells were cultured in OPTIMEM medium with 1% GlutaMAX and 1% Hepes (GIBCO) supplemented with 10 ng/mL Epidermal Growth Factor (EGF, PMG8041, Thermo Fisher Scientific) and 1% P/S. All cells were

cultured at 37°C in 5% CO_2 incubator and media were changed every 48 h and passages were done at 90% of confluence.

3.2.1.2. Organoids

Epithelial primary cells, isolated from colons of patients, were cultured as colonoids. Sample 1 was obtained from a woman (born in 1956) left colon laparoscopic resection (treatment of a sigmoido-vaginal fistula for diverticulitis); sample 2 was collected from a woman (born in 1955) left colon laparoscopic resection (treatment for recurrent diverticulitis); sample 3 was taken from a man (born in 1938) sigmoid laparoscopic resection (treatment for fistulized sigmoiditis); sample 4 has been taken from a man (born in 1965) well-differentiated colonic (caecum) adenocarcinoma, infiltrating the serosa with numerous (>7) lymph node metastases, stage pT4N2b (advanced stage III), abnormal somatic phenotype: loss of expression of hMSH2 and hMSH6 proteins, microsatellite instability (MSI) (suspicion of Lynch syndrome) and sample 5 was collected from a man (born in 1959) with colonic adenocarcinoma (right colon) who had undergone nine courses of chemotherapy. Human colonic tissues were obtained from individuals treated at the Centre Hospitalier de Toulouse (France). The written and verbal informed consent was obtained before enrolment in the study, and the Ethics Committee approved the human research protocol (ClinicalTrials.gov identifiers: NCT01990716 and RC31/21/0038).

Colonic epithelial cells were isolated and cultured as organoids in the ORGANOIDS platform of the IRSD (Institute of digestive health research) in Toulouse, as previously described [83]. Samples 1 to 3 are used as controls compared to tumor samples 4 and 5. 50 colonic crypts seeded in 25 µl Matrigel® (hESC-qualified, BD Biosciences) by well of 48 wells plate were incubated at 37°C in a 5% CO_2 and proliferate as organoids (normal tissue) or spheroids (tumor tissue) in the presence of the following medium: Advanced DMEM/F12 (Invitrogen, 12634-010), 2 mM Glutamax (Invitrogen, A1286001), 10 mM hepes (Gibco, 15630-056), 1X N2 (Invitrogen, 17502-048), 1X B27 minus vitamin A (Life technologies, 12587-010), 50 ng/ml human EGF (Gibco, PHG0314), 100 ng/ml human noggin (Tebu, 120-10C), 48% Wnt3a conditioned medium, 1 µg/ml human R-spondin (R&D Systems, 4645RS), 10 mM nicotinamide (Sigma Aldrich, N0636), 10 nM gastrin (Sigma Aldrich, G9145-1MG), 10 µM SB202190 (Sigma Aldrich, 57067), 0.01 µM PGE2 (Sigma Aldrich, P0409-1MG). At day 0 only, 10 µM Y27632 (Sigma Aldrich, Y0503), 0.5 µM LY2157299 (Axon MedChem, 1941), and 1 mM N-acetylcysteine (Sigma Aldrich, A9165-5G) were added.

To amplify the cellular material, around 3 passages in new Matrigel® were realized after 8 days of primo-culture. 250 µl Cell recovery solution (Corning) was added in culture wells and plates were maintained on ice during 20 min to dissociate 3D cellular structures from Matrigel®. After, wells from the same sample were collected in 14 ml of Advanced DMEM/F12 *plus* Glutamax and hepes, and centrifuged (1000 rpm, 3 min, 4°C). Supernatant was discarded and 5 ml of TrypLE express (Invitrogen) was added and incubated for 5 min at 37°C to obtain individual cells by repetitive pipetting. After addition of 25 ml of Advanced DMEM/F12 *plus* Glutamax/hepes and 2.5% fetal calf serum (Gibco), and centrifugation (1500 rpm, 3 min, 4°C), Matrigel® was added on the pellet. Cells resuspended in Matrigel® were seeded in new wells of 48 wells plate and cultured as above during 8 days. After 3 passages, organoids and spheroids were frozen. For freezing, 3D structures were dissociated from Matrigel® by Cell recovery solution as described above and directly frozen in 500 µl Synth-a-Freeze medium (Thermo Fisher Scientific). Then, organoids and spheroids conserved in liquid N_2 were unfrozen and cultured in Matrigel® as described above for 1 week before their use in cytotoxicity tests. For cytotoxicity test, organoids and spheroids were dissociated from Matrigel® with 500 µL/well of trypsin and individual cells were seeded in Matrigel® on 96-wells plates (Thermo Fisher Scientific) and allowed to proliferate as colonoids.

3.2.1.3. Cytotoxicity tests

Forty-eight hours before cytotoxicity test, 2500 (organoid assay) or 40 000 (Caco-2 assay) or 60 000 (HIEC6 assay) cells/well were seeded in 96-wells plates (Thermo Fisher Scientific). Compounds **1**-**7** were dissolved in dimethyl sulfoxide (DMSO, Thermo Fisher Scientific) at 10 mg/mL, followed by successive dilutions with medium to obtain final concentrations. At 48 h after cells seeding, daphnanes were added in triplicates with DMSO as a control (maximum concentration 0.01%). After 48 h, MTS (Cell line assay, CellTiter 96 AQueous One Solution Cell Proliferation Assay, Promega) or CellTiter-Glo (Organoid assay, Luminescent Cell Viability Assay, Promega) were added on each well and cytotoxicity tests were performed according to the manufacturer's instructions. Then, cell viability was measured by colorimetry at 490 nm for MTS or by luminescent measure for CellTiter-Glo (Varioskan Flash and logiciel SkanIT RE 2.4.3, Thermo Fisher Scientific). For some tests, atypical PKCs inhibitor CRT0066854 hydrochloride (0.625, 1.25 or 2.5 µM, Tocris Bioscience), PKCα inhibitor Gö6976 (0.2 µM, Calbiochem) and MEK inhibitor PD-0325901 (0.5 µM, MedChemExpress) were added 30 minutes (atypical PKCs inhibitor) or 15 minutes (PKCα and MEK inhibitors) before daphnanes (maximum concentration of DMSO 0,015%).

For the tests on organoids, 5-Fluoro-2'-deoxyuridine (Floxuridin, FUdR, Sigma-Aldrich, Ref F0503) at 1 µg/mL was used as positive control. It was dissolved in 50 mM Phosphate Buffer Saline (PBS, GIBCO) and diluted to obtain the final concentration.

~~*3.2.1.4. Microscopic analysis*~~

~~Cells culture evolution before and after treatment was monitored daily with phase contrast optical microscope (10x objective, Nikon Eclipse TS2 microscope) and pictures were taken 48 h after treatment (Nikon camera and N/S Element software).~~

3.2.1.4. Immunofluorescence and confocal analysis

40 000 Caco-2 cells were seeded in a 96-well plate and treated as for cytotoxicity tests. After 48 h of treatment, medium was removed and cells were fixed with 15 µL of paraformaldehyde (PFA 3.7%, Sigma Aldrich) during 20 min at room temperature. After washing with 100 µL HBSS (GIBCO), cells were permeabilized with 50 µL HBSS/Triton X100 0.5% *plus* Bovine Serum Albumin (BSA, Dutscher) 1% for 15 min at room temperature. To study the expression and localization of PKCζ and PKCα, Caco-2 cells were then incubated primary antibodies (anti-PKCζ SC-17781 Santa Cruz Biotechnology, 1/50 or anti-PKCα Ab32376 Abcam, 1/200) diluted in permeation buffer, overnight at 4°C. After 3 washes for 10 min, secondary antibodies (Alexa fluor 488 goat anti-mouse, Life Technologies, 1/1000 or Alexa fluor 488 goat anti-rabbit, Invitrogen, 1/1000) diluted in permeation buffer, were added during 45 min at room temperature in dark. After 3 washes, 50 µL of phalloidin fluor 568 (33 nM) *plus* Hoechst 3342 (5 µg/ml) or Rhodamine Phalloidin reagent (R415, Invitrogen, Thermo Fisher Scientific, 1/500), diluted in permeation buffer was added in each well during 30 min at room temperature in dark. After 3 washes, in some assays Prolong reagent with DAPI (Invitrogen, Thermo Fisher Scientific) was added. Analysis by confocal microscopy was performed with Opera Phenix Plus High-Content Screening PerkinElmer (Harmony software) or LSM710 Zeiss (Zen software). Pictures were analyzed and quantified by ImageJ software (Image Processing and Analysis in Java).

3.2.1.5. Western blot

To investigate the impact of daphnanes on signaling pathways, PKCζ and PKCδ in Caco-2 cells, Western blot protein analyses were performed. Caco-2 cells ($0.25x10^6$ cells/well) were seeded in 12-well plate (Thermo Fisher Scientific) in 1 mL of medium and treated as for cytotoxicity tests. After 48 h of treatment, medium was removed and cells were

washed twice with 1 mL PBS supplemented with calcium and magnesium. Cells were lysed on ice with 50 µL of pH 7.4 lysis buffer (containing: Tris HCl 50 mM, NaCl 150 mM, Triton X100 0,1%, EDTA 1 mM) supplemented with proteases inhibitor (1/25, Complete mini EDTA free Roche) and phosphatases inhibitor (1/100, Inhibitor cocktail 2, Sigma Aldrich). Lysates were collected with a Cell Scrapper (Sarstedt) and stored at 4°C.

Thirty micrograms of protein were mixed with Laemmli buffer (Bio-Rad) containing Sodium Dodecyl Sulfate/glycerol/bromophenol blue/β-mercaptoethanol to a final volume of 15 µL heated at 95°C for 5 min (ThermoMixer F1.5, Eppendorf) to denature the proteins. Each sample was resolved on 4 to 15% precast acrylamide gel (Mini-PROTEAN, TGX, Bio-Rad) and transferred to nitrocellulose membrane (Bio-Rad). After saturation with PBS/milk 5%/BSA 1% for 1 h, membrane was probed overnight at 4°C with the appropriate primary antibody diluted in PBS/milk 1%/BSA 0.2%. Primary antibodies were obtained from Cell signaling technology (phospho MEK1/2 (Ser217/221) #41G9, MEK1/2 #L38C12, phospho Akt (Ser473) #4060); Abcam (β-catenin #AB32572, phospho-PKCδ #AB5658); Santa Cruz biotechnology (phospho PKCζ (Thr410) #SC-271962, PKCζ #SC-17781, Akt #SC-8312, PKCδ #SC937), Sigma Aldrich (phopho GSK3β (Ser9) #04-1075) and BD transduction laboratories (GSK3β #610202). After 3 washes with PBS/0.2% Tween 20 for 10 min, membrane was incubated with appropriate secondary antibody (anti-mouse HRP or anti-rabbit HRP) for 90 min at room temperature. Detection was achieved using Enhanced ChemiLuminescence (ECL, Clarity Max or Clarity, Bio-Rad) reagent and visualized on Molecular Imager ChemiDoc XRS (Bio-Rad) with ImageLab software.

3.2.1.7. Statistical analysis

Statistical analyses were performed using GraphPad Prism 7. Student's *t*-test and 2way ANOVA test were used for experiments analysis. P values < 0.05 were considered to be significant.

3.2.2. Evaluation of the antiviral activity of isolated mono-esterified daphnanes

3.2.2.1. Cell and virus cultures

Human lung epithelial A549 cell line overexpressing human ACE2 and TMPRSS2 proteins was purchased from Invivogen (Toulouse, France) and maintained in DMEM supplemented with 10% FBS, 1% penicillin/streptomycin, 0.1% amphotericin B (PAN Biotech), 100 µg/mL hygromycin, 0.5 µg/mL puromycin, 10 µg/mL blasticidin and 100

μg/mL zeocin. Vero cells were purchased from ATCC and cultured in Essential Minimal Eagle's Medium (MEM, PAN Biotech) containing 5% FBS, 1% penicillin/streptomycin and 0.1% amphotericin B. All cells were cultured at 37°C in 5% CO_2 incubator. SARS-CoV-2 virus was isolated in 2020 from a nasopharyngeal swab from a COVID-19 PCR-positive patient in Reunion Island. The recombinant Zika virus expressing the GFP reporter gene ($ZIKV^{GFP}$) was obtained as previously described [84].

3.2.2.2. Antiviral assays

To determine the antiviral activity of compounds against SARS-CoV-2, $A549^{ACE2\ and\ TMPRSS2}$ overexpressing cells seeded in 24-well plates were incubated with different concentrations of each compound, starting from its maximal non-cytotoxic concentration (MNTC), and infected with SARS-CoV-2 at a multiplicity of infection (MOI) of 0.001. Twenty-four hours after infection, supernatant was harvested to titrate viral growth *via* plaque forming units assays (PFU). To determine the antiviral activity of compounds against Zika virus, cells seeded in 96-well plates were incubated with different concentrations of each compound, starting from 50 μg/mL, and infected with ZIKVGFP at a multiplicity of infection (MOI) of 1. Twenty-four hours post-infection, cells were harvested, fixed with 3.7% PFA in PBS for 20 min, washed twice with PBS and then subjected to flow cytometric analysis using Cytoflex (Beckman). Results were analyzed using Cytexpert software.

3.2.2.3. Viral titration

Supernatants obtained from 24 h SARS-CoV-2 infected cells were harvested and stored at -80°C for PFU assay. A 70% confluent monolayer of VeroE6 cells in 24-wells plate was incubated during 2 h with 100 μL of a ten-fold serial dilution of the supernatants. Then, MEM containing 1% carboxymethyl cellulose (CMC) was added to each well and incubated at 37°C under 5% CO_2. Three days later, infected cells were carefully washed twice with PBS and fixed for 10 min with 4% PFA. Then, cells were washed and stained with crystal violet. Plaques were counted and expressed as PFU/mL.

4. Funding information

This work was supported by the French Ministry of Higher Education and Research (three years PhD grant) and by the financial support from the region Occitanie.

Declaration of Competing Interest

The authors declare that they have no known competing financial interests or personal relationships that could have appeared to influence the work reported in this paper.

Acknowledgements

We would like to thank Celine Deraeve (LCC) for access to the IR spectrometer, Charles-Louis Serpentini (IMRCP) for access to the ECD spectrometer, and Pierre Lavedan, Marc Vedrenne and Caroline Toppan from the NMR platform of the Institut de Chimie de Toulouse (ICT) for NMR analyses. We thank the Organoid Platform at the Institut de Recherche en Santé Digestive (INSERM, Toulouse, France) for help with confocal microscopy and/or image analysis (https://www.irsd.fr/organoides.html), the department of digestive surgery (Toulouse University Hospital) for samples from patients, Pr Elmostafa Barahoui (INFINITY, Toulouse) for discussion along PKC investigations and gift of PKCδ antibodies, and Dr Mireille Sebbag (IRSD, Toulouse) for advices in human organoids cell viability assays.

Appendix A. Supplementary material

References

1. Ramalho S, Pinto M, Ferreira D, Bolzani V. Biologically Active Orbitides from the Euphorbiaceae Family. Planta Med. 2018;84:558‐67. https://doi.org/10.1055/s-0043-122604.

2. Bijekar S, Gayatri M. Ethanomedicinal properties of Euphorbiaceae family- A comprehensive review. Int J Phytomedicine. 2014;6:144‐56.

3. Mwine JT, Damme PV. Why do Euphorbiaceae tick as medicinal plants? A review of Euphorbiaceae family and its medicinal features. J Med Plant Res. 2011;5:652‐62.

4. Tobias LM, Cordeiro I, Demarco D. Floral development in Hura crepitans (Euphorbiaceae): a bat-pollinated species with multicarpellate gynoecium. Braz J Bot. 2019;42:509‐19. https://doi.org/10.1007/s40415-019-00543-0.

5. Owojuyigbe OS, Firempong CK, Larbie C, Komlaga G, Emikpe BO. Hepatoprotective Potential of Hura crepitans L.: A Review of Ethnomedical, Phytochemical and Pharmacological Studies. J Complement Altern Med Res. 2020;9:1‐10. https://doi.org/10.9734/jocamr/2020/v9i230136.

6. Kadiri AB, Adeniran S. Study of the anatomy of the genus Hura L. (Euphorbiaceae). Ife Jounal Sci. 2016;18:413‐26.

7. Hura cepitans L., 1753 [Internet]. Inventaire national du patrimoine naturel. 2003 [cited on 28 July 2022]. Available on: https://inpn.mnhn.fr/espece/cd_nom/629870.

8. Trinel M, Jullian V, Le Lamer AC, Mhamdi I, Mejia K, Castillo D, et al. Profiling of *Hura crepitans* L. latex by ultra-high-performance liquid chromatography/atmospheric pressure chemical ionisation linear ion trap Orbitrap mass spectrometry. Phytochem Anal. 2018;29:627‑38. https://doi.org/10.1002/pca.2776.

9. Remy S, Litaudon M. Macrocyclic Diterpenoids from Euphorbiaceae as A Source of Potent and Selective Inhibitors of Chikungunya Virus Replication. Molecules. 2019;24:1‑16. https://doi.org/10.3390/molecules24122336.

10. Vasas A, Hohmann J. *Euphorbia* Diterpenes: Isolation, Structure, Biological Activity, and Synthesis (2008–2012). Chem Rev. 2014;114:8579‑612. https://doi.org/10.1021/cr400541j.

11. Buchanan JG, Crews P, Epe B, Evans FJ, Hanke FJ, Manes LV, et al. Fortschritte der Chemie organischer Naturstoffe / Progress in the Chemistry of Organic Natural Products. Springer. Vol. 44. Vienna: Springer Vienna; 1983. 333 p. https://doi.org/10.1007/978-3-7091-8714-2.

12. Shi QW, Su XH, Kiyota H. Chemical and Pharmacological Research of the Plants in Genus *Euphorbia*. Chem Rev. 2008;108:4295‑327. https://doi.org/10.1021/cr078350s.

13. Olivon F, Remy S, Grelier G, Apel C, Eydoux C, Guillemot JC, et al. Antiviral Compounds from *Codiaeum peltatum* Targeted by a Multi-informative Molecular Networks Approach. J Nat Prod. 2019;82:330‑40. https://doi.org/10.1021/acs.jnatprod.8b00800.

14. Nothias-Scaglia LF, Pannecouque C, Renucci F, Delang L, Neyts J, Roussi F, et al. Antiviral Activity of Diterpene Esters on Chikungunya Virus and HIV Replication. J Nat Prod. 2015;78:1277‑83. https://doi.org/10.1021/acs.jnatprod.5b00073.

15. Nothias-Scaglia LF, Dumontet V, Neyts J, Roussi F, Costa J, Leyssen P, et al. LC-MS2-Based dereplication of Euphorbia extracts with anti-Chikungunya virus activity. Fitoterapia. 2015;105:202‑9. http://dx.doi.org/10.1016/j.fitote.2015.06.021.

16. Bourjot M, Leyssen P, Neyts J, Dumontet V, Litaudon M. Trigocherrierin A, a Potent Inhibitor of Chikungunya Virus Replication. Molecules. 2014;19:3617‑27. https://doi.org/10.3390/molecules19033617.

17. Rashad AA, Mahalingam S, Keller PA. Chikungunya Virus: Emerging Targets and New Opportunities for Medicinal Chemistry. J Med Chem. 2014;57:1147‑66. http://dx.doi.org/10.1021/jm400460d.

18. Yan M, Lu Y, Chen CH, Zhao Y, Lee KH, Chen DF. Stelleralides D–J and Anti-HIV Daphnane Diterpenes from *Stellera chamaejasme*. J Nat Prod. 2015;78:2712‑8. https://doi.org/10.1021/acs.jnatprod.5b00660.

19. Lai W, Huang L, Zhu L, Ferrari G, Chan C, Li W, et al. Gnidimacrin, a Potent Anti-HIV Diterpene, Can Eliminate Latent HIV-1 Ex Vivo by Activation of Protein Kinase C β. J Med Chem. 2015;58:8638‑46. https://doi.org/10.1021/acs.jmedchem.5b01233.

20. Nothias-Scaglia LF, Retailleau P, Paolini J, Pannecouque C, Neyts J, Dumontet V, et al. Jatrophane Diterpenes as Inhibitors of Chikungunya Virus Replication: Structure–Activity Relationship and Discovery of a Potent Lead. J Nat Prod. 2014;77:1505‐12. https://dx.doi.org/10.1021/np500271u.

21. Kostelecky B. An Investigation of PKC Isoform Functional Specificity [Thesis]. [London]: University College London; 2009.

22. Isakov N. Protein kinase C (PKC) isoforms in cancer, tumor promotion and tumor suppression. Semin Cancer Biol. 2018;48:36‐52. http://dx.doi.org/10.1016/j.semcancer.2017.04.012.

23. Farhadi A, Keshavarzian A, Ranjbaran Z, Fields JZ, Banan A. The Role of Protein Kinase C Isoforms in Modulating Injury and Repair of the Intestinal Barrier. J Pharmacol Exp Ther. 2006;316:1‐7. https://doi.org/10.1124/jpet.105.085449.

24. Rimessi A, Patergnani S, Ioannidi E, Pinton P. Chemoresistance and Cancer-Related Inflammation: Two Hallmarks of Cancer Connected by an Atypical Link, PKCζ. Front Oncol. 2013;3:1‐7. https://doi.org/10.3389/fonc.2013.00232.

25. Linch M, Sanz-Garcia M, Rosse C, Riou P, Peel N, Madsen CD, et al. Regulation of polarized morphogenesis by protein kinase C iota in oncogenic epithelial spheroids. Carcinogenesis. 2014;35:396‐406. https://doi.org/10.1093/carcin/bgt313.

26. St Johnston D, Sanson B. Epithelial polarity and morphogenesis. Curr Opin Cell Biol. 2011;23:540‐6. https://doi.org/10.1016/j.ceb.2011.07.005.

27. Reina-Campos M. The Dual Roles of the Atypical Protein Kinase Cs in Cancer. Cancer Cell. 2019;36:218‐35. https://doi.org/10.1016/j.ccell.2019.07.010.

28. Überall F, Hellbert K, Kampfer S, Maly K, Villunger A, Spitaler M, et al. Evidence That Atypical Protein Kinase C-λ and Atypical Protein Kinase C-ζ Participate in Ras-mediated Reorganization of the F-actin Cytoskeleton. J Cell Biol. 1999;144:413‐25.

29. Keenan C, Kelleher D. Protein Kinase C and the Cytoskeleton. Cell Signal. 1998;10:225‐32. https://doi.org/10.1016/S0898-6568(97)00121-6.

30. Garcia MA, Nelson WJ, Chavez N. Cell–Cell Junctions Organize Structural and Signaling Networks. Cold Spring Harb Perspect Biol. 2018;10:1‐27. https://doi.org/10.1101/cshperspect.a029181.

31. Drummond ML, Prehoda KE. Molecular Control of Atypical Protein Kinase C: Tipping the Balance between Self-Renewal and Differentiation. J Mol Biol. 2016;428:1455‐64. http://dx.doi.org/10.1016/j.jmb.2016.03.003.

32. Mukherjee A, Roy S, Saha B, Mukherjee D. Spatio-Temporal Regulation of PKC Isoforms Imparts Signaling Specificity. Front Immunol. 2016;7:1‐7. https://doi.org/10.3389/fimmu.2016.00045.

33. Kawano T, Inokuchi J, Eto M, Murata M, Kang JH. Activators and Inhibitors of Protein Kinase C (PKC): Their Applications in Clinical Trials. Pharmaceutics. 2021;13:1‐27. https://doi.org/10.3390/pharmaceutics13111748.

34. Xi Y, Xu P. Global colorectal cancer burden in 2020 and projections to 2040. Transl Oncol. 2021;14:1‐7. https://doi.org/10.1016/j.tranon.2021.101174.

35. Juanes MA. Cytoskeletal Control and Wnt Signaling—APC's Dual Contributions in Stem Cell Division and Colorectal Cancer. Cancers. 2020;12:1‐21. https://doi.org/10.3390/cancers12123811.

36. Hankey W. Functions of the APC tumor suppressor protein dependent and independent of canonical WNT signaling: implications for therapeutic targeting. Cancer Metastasis Rev. 2018;37:159‐72. https://doi.org/10.1007/s10555-017-9725-6.

37. Zhou G, Yang J, Song P. Correlation of ERK/MAPK signaling pathway with proliferation and apoptosis of colon cancer cells. Oncol Lett. 2018;17:2266‐70. https://doi.org/10.3892/ol.2018.9857.

38. Fang JY, Richardson BC. The MAPK signalling pathways and colorectal cancer. Lancet Oncol. 2005;6:322‐7. https://doi.org/10.1016/S1470-2045(05)70168-6.

39. Vidri RJ, Fitzgerald TL. GSK-3: An important kinase in colon and pancreatic cancers. Biochim Biophys Acta BBA - Mol Cell Res. 2020;1867:1‐4. https://doi.org/10.1016/j.bbamcr.2019.118626.

40. Shakoori A, Ougolkov A, Yu ZW, Zhang B, Modarressi MH, Billadeau DD, et al. Deregulated GSK3β activity in colorectal cancer: Its association with tumor cell survival and proliferation. Biochem Biophys Res Commun. 2005;334:1365‐73. https://doi.org/10.1016/j.bbrc.2005.07.041.

41. Duda P, Akula SM, Abrams SL, Steelman LS, Martelli AM, Cocco L, et al. Targeting GSK3 and Associated Signaling Pathways Involved in Cancer. Cells. 2020;9:1‐28. https://doi.org/ 10.3390/cells9051110.

42. Ma L, Tao Y, Duran A, Llado V, Galvez A, Barger JF, et al. Control of Nutrient Stress-Induced Metabolic Reprogramming by PKCζ in Tumorigenesis. Cell. 2013;152:599‐611. https://doi.org/10.1016/j.cell.2012.12.028.

43. Tejeda-Muñoz N, González-Aguilar H, Santoyo-Ramos P, Castañeda-Patlán MC, Robles-Flores M. Glycogen Synthase Kinase 3β Is Positively Regulated by Protein Kinase Cζ-Mediated Phosphorylation Induced by Wnt Agonists. Mol Cell Biol. 2016;36:731‐41. https://doi.org/10.1128/MCB.00828-15.

44. Llado V, Nakanishi Y, Duran A, Reina-Campos M, Shelton PM, Linares JF, et al. Repression of Intestinal Stem Cell Function and Tumorigenesis through Direct Phosphorylation of β-Catenin and Yap by PKCζ. Cell Rep. 2015;10:740‐54. https://doi.org/10.1016/j.celrep.2015.01.007.

45. Dupasquier S, Blache P, Picque Lasorsa L, Zhao H, Abraham JD, Haigh JJ, et al. Modulating PKCα Activity to Target Wnt/β-Catenin Signaling in Colon Cancer. Cancers. 2019;11:1‐19. https://doi.org/10.3390/cancers11050693.

46. Gwak J, Cho M, Gong SJ, Won J, Kim DE, Kim EY, et al. Protein-kinase-C-mediated β-catenin phosphorylation negatively regulates the Wnt/β-catenin pathway. J Cell Sci. 2006;119:4702‐9. https://doi.org/10.1242/jcs.03256.

47. Lee JM, Kim IS, Kim H, Lee JS, Kim K, Yim HY, et al. RORα Attenuates Wnt/β-Catenin Signaling by PKCα-Dependent Phosphorylation in Colon Cancer. Mol Cell. 2010;37:183‑95. https://doi.org/10.1016/j.molcel.2009.12.022.

48. Ersahin T, Tuncbag N, Cetin-Atalay R. The PI3K/AKT/mTOR interactive pathway. Mol Biosyst. 2015;11:1946‑54. https://doi.org/ 0.1039/C5MB00101C.

49. Oster H, Leitges M. Protein Kinase C α but not PKCζ Suppresses Intestinal Tumor Formation in *ApcMin/+* Mice. Cancer Res. 2006;66:6955‑63. https://doi.org/10.1158/0008-5472.CAN-06-0268.

50. Trinel M, Le Lamer AC, Jullian V, Jacquemin D, Graton J, Cristofoli V, et al. Daphnanes diterpenes from the latex of Hura crepitans L. And activity against human colorectal cancer cells Caco-2. Bioorganic Chem. 2020;103:1‑13. https://doi.org/10.1016/j.bioorg.2020.104132.

51. Smith SG, Goodman JM. Assigning Stereochemistry to Single Diastereoisomers by GIAO NMR Calculation: The DP4 Probability. J Am Chem Soc. 2010;132:12946‑59. https://doi.org/10.1021/ja105035r.

52. Jin YX, Shi LL, Zhang DP, Wei HY, Si Y, Ma GX, et al. A Review on Daphnane-Type Diterpenoids and Their Bioactive Studies. Molecules. 2019;24:1‑14. https://doi.org/10.3390/molecules24091842.

53. Otsuki K, Li W, Miura K, Asada Y, Huang L, Chen CH, et al. Isolation, Structural Elucidation, and Anti-HIV Activity of Daphnane Diterpenoids from *Daphne odora*. J Nat Prod. 2020;83:3270‑7. https://doi.org/10.1021/acs.jnatprod.0c00540.

54. Noah TK, Donahue B, Shroyer NF. Intestinal development and differentiation. Exp Cell Res. 2011;317:2702‑10. https://doi.org/10.1016/j.yexcr.2011.09.006.

55. Aran V, Victorino AP, Thuler LC, Ferreira CG. Colorectal Cancer: Epidemiology, Disease Mechanisms and Interventions to Reduce Onset and Mortality. Clin Colorectal Cancer. 2016;15:195‑203. https://doi.org/10.1016/j.clcc.2016.02.008.

56. Abraham C, Scaglione-Sewell B, Skarosi S.F, Qin W, Bissonnette M, Brasitus T.A. Protein Kinase C a Modulates Growth and Differentiation in Caco-2 Cells. Gastroenterology. 1998;114:503‑9. https://doi.org/10.1016/S0016-5085(98)70533-5.

57. Wald FA, Oriolo AS, Mashukova A, Fregien NL, Langshaw AH, Salas PJI. Atypical protein kinase C (iota) activates ezrin in the apical domain of intestinal epithelial cells. J Cell Sci. 1 mars 2008;121(5):644‑54. https://doi.org/10.1242/jcs.016246.

58. Banan A, Zhang LJ, Shaikh M, Fields JZ, Farhadi A, Keshavarzian A. θ-Isoform of PKC is required for alterations in cytoskeletal dynamics and barrier permeability in intestinal epithelium: a novel function for PKC-θ. Am J Physiol-Cell Physiol. 2004;287(1):218‑34. https://doi.org/ 10.1152/ajpcell.00575.2003.

59. Cerda SR, Mustafi R, Little H, Cohen G, Khare S, Moore C, et al. Protein kinase C delta inhibits Caco-2 cell proliferation by selective changes in cell cycle and cell death regulators. Oncogene. 2006;25(22):3123‑38. https://doi.org/10.1038/sj.onc.1209360.

60. Umar S, Sellin JH, Morris AP. Increased nuclear translocation of catalytically active PKC-ζ during mouse colonocyte hyperproliferation. Am J Physiol-Gastrointest Liver Physiol. 2000;279(1):223‑37. https://doi.org/ 10.1152/ajpgi.2000.279.1.G223.

61. Rickard K.L, Gibson P.R, Wilson N.J, Mariadason J.M, Phillips W.A. Short-Chain Fatty Acids Reduce Expression of Specific Protein Kinase C Isoforms in Human Colonic Epithelial Cells. J Cell Physiol. 2000;182:222‑31. https://doi.org/10.1002/(SICI)1097-4652(200002)182:2<222::AID-JCP11>3.0.CO;2-B.

62. Kjær S, Linch M, Purkiss A, Kostelecky B, Knowles PP, Rosse C, et al. Adenosine-binding motif mimicry and cellular effects of a thieno[2,3-*d*]pyrimidine-based chemical inhibitor of atypical protein kinase C isoenzymes. Biochem J. 2013;451:329‑42. https://doi.org/10.1042/BJ20121871.

63. Xiong X, Li X, Wen YA, Gao T. Pleckstrin Homology (PH) Domain Leucine-rich Repeat Protein Phosphatase Controls Cell Polarity by Negatively Regulating the Activity of Atypical Protein Kinase C. J Biol Chem. 2016;291:25167‑78. https://doi.org/10.1074/jbc.M116.740639.

64. Standaert ML, Bandyopadhyay G, Kanoh Y, Sajan MP, Farese RV. Insulin and PIP_3 Activate PKC-ζ by Mechanisms That Are Both Dependent and Independent of Phosphorylation of Activation Loop (T410) and Autophosphorylation (T560) Sites. Biochemistry. 2001;40:249‑55. https://doi.org/10.1021/bi0018234.

65. Ranganathan S, Wang Y, Kern FG, Zhican Q, Rongbao L. Activation loop phosphorylation-independent kinase activity of human protein kinase C zeta. Poteins Struct Funct Bioinforma. 2007;67:709‑19. https://doi.org/10.1002/prot.21348.

66. Zhang N, Tian YN, Zhou LN, Li MZ, Chen HD, Song SS, et al. Glycogen synthase kinase 3β inhibition synergizes with PARP inhibitors through the induction of homologous recombination deficiency in colorectal cancer. Cell Death Dis. 2021;12:1‑18. https://doi.org/10.1038/s41419-021-03475-4.

67. Liu K, Li J, Wu X, Chen M, Luo F, Li J. GSK-3β inhibitor 6-bromo-indirubin-3′-oxime promotes both adhesive activity and drug resistance in colorectal cancer cells. Int J Oncol. 2017;51:1821‑30. https://doi.org/10.3892/ijo.2017.4163.

68. Umar S, Wang Y, Morris AP, Sellin JH. Dual alterations in casein kinase I-ε and GSK-3β modulate β-catenin stability in hyperproliferating colonic epithelia. Am J Physiol-Gastrointest Liver Physiol. 2007;292:599‑607. https://doi.org/10.1152/ajpgi.00343.2006.

69. Wakatsuki S, Saitoh F, Araki T. ZNRF1 promotes Wallerian degeneration by degrading AKT to induce GSK3B-dependent CRMP2 phosphorylation. Nat Cell Biol. déc 2011;13(12):1415‑23. https://doi.org/10.1038/ncb2373.

70. Monick MM, Carter AB, Flaherty DM, Peterson MW, Hunninghake GW. Protein Kinase C ζ Plays a Central Role in Activation of the p42/44 Mitogen-Activated Protein Kinase by Endotoxin in Alveolar Macrophages. J Immunol. 2000;165:4632‑9. https://doi.org/10.4049/jimmunol.165.8.4632.

71. Carragher LAS, Snell KR, Giblett SM, Aldridge VSS, Patel B, Cook SJ, et al. ^{V600E} Braf induces gastrointestinal crypt senescence and promotes tumour progression through enhanced CpG methylation of *p16* ^{INK4a} . EMBO Mol Med. 2010;2:458‑71. https://doi.org/10.1002/emmm.201000099.

72. Wardana AP, Aminah NS, Rosyda M, Abdjan MI, Kristanti AN, Tun KNW, et al. Potential of diterpene compounds as antivirals, a review. Heliyon. 2021;7:1‑14. https://doi.org/10.1016/j.heliyon.2021.e07777.

73. Liu X, Verma A, Garcia G, Ramage H, Lucas A, Myers RL, et al. Targeting the coronavirus nucleocapsid protein through GSK-3 inhibition. Proc Natl Acad Sci. 2021;118:1‑9. https://doi.org/10.1073/pnas.2113401118.

74. Rana AK, Rahmatkar SN, Kumar A, Singh D. Glycogen synthase kinase-3: A putative target to combat severe acute respiratory syndrome coronavirus 2 (SARS-CoV-2) pandemic. Cytokine Growth Factor Rev. 2021;58:92‑101. https://doi.org/10.1016/j.cytogfr.2020.08.002.

75. Tostivint V, Racaud-Sultan C, Roumiguié M, Soulié M, Gamé X, Beauval J baptiste. Progrès dans l'étude du cancer de la prostate : la culture cellulaire en trois dimensions reproduit ex vivo les caractéristiques des tumeurs prostatiques. Presse Médicale. 2017;46:954‑65. https://doi.org/10.1016/j.lpm.2017.06.014.

76. Multum C. Floxuridine [Internet]. Drugs.com. 2022. [cited on 12 Dec. 2022] Avalaible on : https://www.drugs.com/mtm/floxuridine.html

77. Rackers JA, Wang Z, Lu C, Laury ML, Lagardère L, Schnieders MJ, et al. Tinker 8: Software Tools for Molecular Design. J Chem Theory Comput. 2018;14(10):5273‑89. https://doi.org/10.1021/acs.jctc.8b00529.

78. Tomasi J, Mennucci B, Cammi R. Quantum Mechanical Continuum Solvation Models. Chem Rev. 2005;105(8):2999‑3094. https://doi.org/10.1021/cr9904009.

79. Barone, G., Gomez-Paloma, L., Duca, D., Silvestri, A., Riccio, R., Bifulco, G. Structure validation of natural products by quantum-mechanical GIAO calculations of 13C NMR chemical shifts. Chem Eur J. 2002;8:3233‑9. https://doi.org/10.1002/1521-3765(20020715)8:14<3233::AID-CHEM3233>3.0.CO;2-0.

80. Schreckenbach G, Ziegler T. Calculation of NMR Shielding Tensors Using Gauge-Including Atomic Orbitals and Modern Density Functional Theory. J Phys Chem. 1995;99:606‑11. https://doi.org/10.1021/j100002a024.

81. Smith SG, Goodman JM. Assigning the Stereochemistry of Pairs of Diastereoisomers Using GIAO NMR Shift Calculation. J Org Chem. 2009;74(12):4597‑607. https://doi.org/10.1021/jo900408d.

82. Grimblat N, Zanardi MM, Sarotti AM. Beyond DP4: an Improved Probability for the Stereochemical Assignment of Isomeric Compounds using Quantum Chemical Calculations of NMR Shifts. J Org Chem. 18 déc 2015;80(24):12526‑34. https://doi.org/10.1021/acs.joc.5b02396.

83. d’Aldebert E, Quaranta M, Sébert M, Bonnet D, Kirzin S, Portier G, et al. Characterization of Human Colon Organoids From Inflammatory Bowel Disease Patients. Front Cell Dev Biol. 2020;8:1‐ 13. https://doi.org/10.3389/fcell.2020.00363.

84. Gadea G, Bos S, Krejbich-Trotot P, Clain E, Viranaicken W, El-Kalamouni C, et al. A robust method for the rapid generation of recombinant Zika virus expressing the GFP reporter gene. Virology. 2016;497:157‐ 62. https://doi.org/10.1016/j.virol.2016.07.015.